INTERNATIONAL JOURNAL FOR NUMERICAL METHODS IN FLUIDS
Int. J. Numer. Meth. Fluids (2009)
Published online in Wiley InterScience (www.interscience.wiley.com). DOI: 10.1002/fld.2139

3D simulation of radionuclide transport in porous media

Fabien Marpeau[1,*,†] and Mazen Saad[2]

[1]*Department of Mathematics (606 PGH), University of Houston, 4800 Calhound Rd., Houston TX 77004, U.S.A.*
[2]*École Centrale de Nantes, Laboratoire de mathématiques Jean Leray (UMR 6629 CNRS), 1 rue de la Noë, BP 92101–44321 Nantes Cedex 3, France*

SUMMARY

We present an efficient and easily implementable finite volume method simulating radionuclide transport through highly heterogeneous grounds in three space dimensions. The numerical concentration of the transported chemicals are proved to remain nonnegative and stable.

Then, we run a realistic test case in which some radioactive iodine I^{129} particles are released from a leak in an underground nuclear waste disposal site. The question of whether the radionuclide invades the underground and reach the ground surface is investigated.

Because of the 3D nature of the problem, a particular emphasis is made on the control of CPU time.

Received 18 June 2008; Revised 11 May 2009; Accepted 20 June 2009

KEY WORDS: porous media flow; transport of contaminant; three space dimensions; numerical simulation; finite volumes; advection–diffusion-reaction

1. INTRODUCTION

While the interest in atom splitting technology keeps constantly growing, underground nuclear waste storage has been more and more considered as a threat. The issue people are getting aware of is that the radionuclides that require to be stored usually have a very long life span and remain dangerous for millions of years. In the meantime, nuclear waste disposal sites might undergo geological constraints due to any kind of Earth's activity, possibly resulting in fractures or leaks in some of the containers in which radioelements are locked in.

Underground nuclear waste disposal sites might be created shortly in Europe. In France, a safety study began about 10 years ago to consider implementing a storage site in the North of

*Correspondence to: Fabien Marpeau, Department of Mathematics (606 PGH), University of Houston, 4800 Calhound Rd., Houston TX 77004, U.S.A.
†E-mail: marpeau@math.uh.edu

Contract/grant sponsor: GNR MoMaS, CNRS, France

the country. Indeed, as real time/scale experiments would last too long and be harmful to the environment, the numerical simulation seems to be an appropriate tool to handle a part of that study. For this purpose, the research group MoMaS (CNRS, France, *cf.* [1]) has been in charge to develop numerical methods, simulates various phenomenons that may happen in and around a site, and test feasibility of radionuclide storage.

In this paper, we assume that a leak occurs in a disposal site, and set up a numerical method simulating the motion of the escaped radionuclides through the underground along time. In particular, a relevant question is whether the radionuclides can invade an underground region and eventually reach the ground surface, constituting a danger for populations living thereon. Several works have been published about this matter (see [2–7], and their references). The main feature of the present work is that the domain of simulation is 3D, which is a realistic way of modeling a ground. However, this main feature is also the main difficulty. Indeed, care must be taken on the control of computation time, which might become extremely long otherwise. Further difficulties include the presence of multiple transport phenomena in the model, and great heterogeneities of geological data that realistic grounds usually feature.

The outline of the paper is the following: our mathematical model is presented in Section 2. This model features an elliptic equation modeling ground water flow and a parabolic equation modeling the displacemnt of radioactive contaminant through the flow. This system is closed by assuming that the ground water is incompressible. In the third section, our numerical strategy is described schematically. The details of the numerical schemes are provided in Section 4. The method is constructed so as to provide nonnegative contaminant concentrations. Section 5 presents a realistic numerical simulation, as an application of our numerical method. The computational effort that was necessary to perform this test is analyzed in Section 6 is an analysis. The end of the paper is composed of a conclusion and technical appendix.

2. MODEL

Let a space domain $\Omega \subset \mathbb{R}^3$ be a saturated porous medium representing a 3D ground. The ground water flow is characterized by its velocity, V, and hydrodynamic load, H. A radionuclide with concentration c is transported through this flow. A widely used PDE system modeling these phenomena (*cf.* [8, 9] and their references) is:

$$\omega(X)\partial_t c(t,X) + \operatorname{div}(c(t,X)V(X)) - \operatorname{div}(D(X,V(X))\nabla c(t,X)) + \lambda\omega(X)c(t,X) = f(t,X) \quad (1)$$

$$V(X) = -K(X)\nabla H(X) \quad (2)$$

$$\operatorname{div} V(X) = 0 \quad (3)$$

with $t \in \mathbb{R}_+$ and $X = (x, y, z) \in \Omega$ denoting time and space independent variables. This system is added an initial condition at $t = 0$ and appropriate boundary conditions on $\partial\Omega$ that will be specified later.

The unknowns of this system are $c \in \mathbb{R}$, $H \in \mathbb{R}$ and $V = (u, v, w) \in \mathbb{R}^3$. Equation (1) models the radionuclide transport, Equation (2) is Darcy's law, and Equation (3) is the incompressibility assumption of the ground water.

In Equation (1), the positive coefficient ω is the product of the porosity of the medium, the solubility of the chemical and retardation factor due to linear adsorption. The positive coefficient λ

DOI: 10.1002/fld

is the radioactive decay factor due to atom splitting, and the nonnegative function f is the source of contaminant coming from the leak in the nuclear waste disposal site. The diffusion–dispersion tensor in (1) is defined by

$$D(X,V)=d_m(X)I+|V|(\alpha_l(X)E(V)+\alpha_t(X)(I-E(V)))$$

where the nonnegative coefficients $d_m,\ \alpha_l,\ \alpha_t$ are the effective diffusion, longitudinal mechanical dispersion and transversal mechanical dispersion coefficients, respectively, I is the three dimensional identity matrix, and

$$E(V)=\frac{1}{|V|^2}\begin{pmatrix} u^2 & uv & uw \\ uv & v^2 & vw \\ uw & vw & w^2 \end{pmatrix} \quad \text{for all } V=(u,v,w)$$

In Equation (2), $K\in\mathbb{R}_+$ denotes the effective permeability of the ground.

We assume that the boundary conditions are constant in time and the presence of radionuclide does not impact the flow. This way, H and V are independent of t. In the following, we come up with numerical methods discretizing (1)–(3) with providing nonnegative and stable concentrations.

3. APPROXIMATION STRATEGY

3.1. Notations and mesh

Throughout the paper, the domain Ω is the parallelepiped $[0,L_x]\times[0,L_y]\times[0,L_z]$, with $L_x,\ L_y$ and L_z being three positive constants. It is discretized with a regular mesh composed of parallelepiped cells. Our interest is to perform far-field simulations over very large space domains. By contrast, the size of the disposal site is very small, and therefore, the support that the source term f is acting in is very localized in space, compared with the whole domain. Indeed, the mesh must be very fine in and around the disposal site so as to capture the source term accurately, whereas for computation time restriction purposes it shall not be reasonable to use a very fine mesh over the whole 3D domain. Thus, we decide to use mesh refinements in each direction. More precisely, we let $N_x\in\mathbb{N}$ be the number of subdivisions of L_x with Δx_i being the ith step in the x-direction for $i=1,\ldots,N_x$. In the same way, we define N_y and N_z with Δy_j and Δz_k being, respectively, the jth step in the y-direction and the kth step in the z-direction, for $j=1,\ldots,N_y,\ k=1,\ldots,N_z$. The interval $(0,T)$ is partitioned into subintervals (t_n,t_{n+1}) and the time steps are defined by $\Delta t_n=t_{n+1}-t_n$. When no confusion arises, Δt_n will be denoted by Δt.

The meshpoints $X_{i,j,k}=(x_i,y_j,z_k)$ are the centroids of the cells $Q_{i,j,k}$, with

$$Q_{i,j,k}=(x_{i-\frac{1}{2}},x_{i+\frac{1}{2}})\times(y_{j-\frac{1}{2}},y_{j+\frac{1}{2}})\times(z_{k-\frac{1}{2}},z_{k+\frac{1}{2}})$$

$$x_{i-\frac{1}{2}}=\sum_{l=1}^{i-1}\Delta x_l,\quad y_{j-\frac{1}{2}}=\sum_{l=1}^{j-1}\Delta y_l,\quad z_{k-\frac{1}{2}}=\sum_{l=1}^{k-1}\Delta z_l$$

$$x_i=x_{i-\frac{1}{2}}+\frac{1}{2}\Delta x_i,\quad y_j=y_{j-\frac{1}{2}}+\frac{1}{2}\Delta y_j,\quad z_k=z_{k-\frac{1}{2}}+\frac{1}{2}\Delta z_k$$

DOI: 10.1002/fld

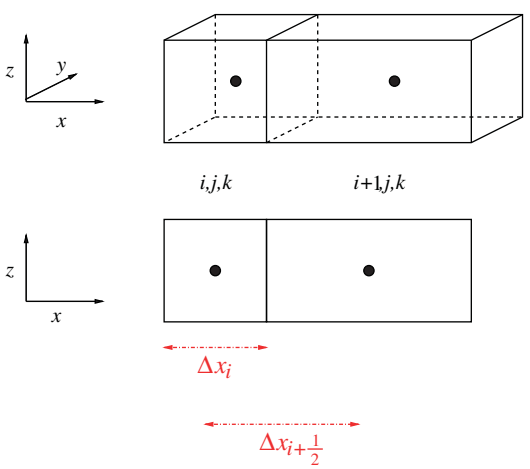

Figure 1. Mesh notations in the x-direction.

We also denote the distances between two meshpoints by $\Delta x_{i+\frac{1}{2}} = x_{i+1} - x_i$, $\Delta y_{j+\frac{1}{2}} = y_{j+1} - y_j$, $\Delta z_{k+\frac{1}{2}} = z_{k+1} - z_k$, see Figure 1. The boundary of $Q_{i,j,k}$ is denoted by: $\partial Q_{i,j,k} = \Gamma_{i+\frac{1}{2},j,k} \cup \Gamma_{i-\frac{1}{2},j,k} \cup \Gamma_{i,j+\frac{1}{2},k} \cup \Gamma_{i,j-\frac{1}{2},k} \cup \Gamma_{i,j,k+\frac{1}{2}} \cup \Gamma_{i,j,k-\frac{1}{2}}$, where $\Gamma_{i+\frac{1}{2},j,k}$ is the shared face between the cells $Q_{i,j,k}$ and $Q_{i+1,j,k}$, $\Gamma_{i,j+\frac{1}{2},k}$ is the shared face between the cells $Q_{i,j,k}$ and $Q_{i,j+1,k}$ and $\Gamma_{i,j,k+\frac{1}{2}}$ is the shared face between the cells $Q_{i,j,k}$ and $Q_{i,j,k+1}$.

For every function ξ defined on $\mathbb{R}_+ \times \Omega$, the notation $\xi^n_{\alpha,\beta,\gamma}$ stands for the approximation of $\xi(t_n, (x_\alpha, y_\beta, z_\gamma))$, for $\alpha = i, i \pm \frac{1}{2}$, $\beta = j, j \pm \frac{1}{2}$, $\gamma = k, k \pm \frac{1}{2}$. Moreover, we denote ξ^n as the sequence $\{\xi^n_{i,j,k}\}_{i,j,k}$.

3.2. *Algorithm*

At the beginning, the constant in time hydrodynamic load H is calculated by combining Equations (2) and (3) as follows:

$$\operatorname{div}(K(X)\nabla H(X)) = 0 \tag{4}$$

Once H is known, the velocity V is then computed from Equation (2). The details of the discretization are provided in Section 4.1.

Once V is known, the concentration c is calculated from Equation (1), which contains two kinds of differential operators: a convection operator and a reaction/diffusion operator. These two operators are isolated by splitting Equation (1) into

$$\omega \partial_t c + \operatorname{div}(cV) = 0 \tag{5}$$

$$\omega \partial_t c - \operatorname{div}(D(X, V)\nabla c) + \omega \lambda c = f \tag{6}$$

DOI: 10.1002/fld

Then, the approximation of c^{n+1} is obtained from c^n by using Strang's splitting algorithm, *cf.* [10]:

$$c^{n+1} = \mathscr{S}_1\left(\frac{\Delta t}{2}, \mathscr{S}_2\left(\Delta t, \mathscr{S}_1\left(\frac{\Delta t}{2}, c^n\right)\right)\right)$$

where $\mathscr{S}_1$ and $\mathscr{S}_2$ are approximation schemes for (5) and (6), respectively. This technique allows us to develop specific numerical schemes that are adapted to each operator. The time step Δt is restricted by a CFL condition providing stability of the explicit scheme $\mathscr{S}_1$. The scheme $\mathscr{S}_2$ is implicit and does not require such a time-step selection. The details of the discretization are expounded in Sections 4.2 and 4.3.

4. NUMERICAL SCHEMES

4.1. Discretization of Darcy's equation

The aim of this section is to approximate the filtration velocity V. The first step consists of calculating the hydrodynamic load H with a finite volume technique. Integrating (4) and using Stoke's formula over any cell $Q_{i,j,k}$ yields:

$$\begin{aligned}
&\int_{\Gamma_{i+\frac{1}{2},j,k}} K(X)\partial_x H(X)\,\mathrm{d}y\,\mathrm{d}z - \int_{\Gamma_{i-\frac{1}{2},j}} K(X)\partial_x H(X)\,\mathrm{d}y\,\mathrm{d}z \\
&\quad + \int_{\Gamma_{i,j+\frac{1}{2},k}} K(X)\partial_y H(X)\,\mathrm{d}x\,\mathrm{d}z - \int_{\Gamma_{i,j-\frac{1}{2},k}} K(X)\partial_y H(X)\,\mathrm{d}x\,\mathrm{d}z \\
&\quad + \int_{\Gamma_{i,j,k+\frac{1}{2}}} K(X)\partial_z H(X)\,\mathrm{d}x\,\mathrm{d}y - \int_{\Gamma_{i,j,k-\frac{1}{2}}} K(X)\partial_z H(X)\,\mathrm{d}x\,\mathrm{d}y = 0
\end{aligned}$$

The derivatives in each direction are discretized by a centered finite difference technique, and H is then approximated at the cell centroids by:

$$\begin{aligned}
&\Delta y_j \Delta z_k \left(K_{i+\frac{1}{2},j,k}\frac{H_{i+1,j,k}-H_{i,j,k}}{\Delta x_{i+\frac{1}{2}}} - K_{i-\frac{1}{2},j,k}\frac{H_{i,j,k}-H_{i-1,j,k}}{\Delta x_{i-\frac{1}{2}}}\right) \\
&+\Delta x_i \Delta z_k \left(K_{i,j+\frac{1}{2},k}\frac{H_{i+1,j,k}-H_{i,j,k}}{\Delta x_{i+\frac{1}{2}}} - K_{i,j-\frac{1}{2},k}\frac{H_{i,j,k}-H_{i-1,j,k}}{\Delta x_{i-\frac{1}{2}}}\right) \\
&+\Delta x_i \Delta y_j \left(K_{i,j,k+\frac{1}{2}}\frac{H_{i,j,k+1}-H_{i,j,k}}{\Delta z_{k+\frac{1}{2}}} - K_{i,j,k-\frac{1}{2}}\frac{H_{i,j,k}-H_{i,j,k-1}}{\Delta z_{k-\frac{1}{2}}}\right) = 0
\end{aligned} \tag{7}$$

The harmonic mean permeability value is preferred to classical interpolation:

$$K_{i+\frac{1}{2},j,k} = \frac{K_{i,j,k}K_{i+1,j,k}\Delta x_i \Delta x_{i+1}}{K_{i,j,k}\Delta x_{i+1} + K_{i+1,j,k}\Delta x_i} \tag{8}$$

In the same way, we define $K_{i,j+\frac{1}{2},k}$ and $K_{i,j,k+\frac{1}{2}}$, respectively, on $\Gamma_{i,j+\frac{1}{2},k}$ and $\Gamma_{i,j,k+\frac{1}{2}}$.

DOI: 10.1002/fld

The numerical scheme (7) involves solving a linear system in the form $AH=L$, where L contains Dirichlet or Neumann boundary conditions, and the matrix A is seven diagonal and strongly dominant. The resolution of this system is carried out by a standard gradient method. In practice (see Section 5), it is crucial that it be pre-conditioned in order to face permeability's sharp gradients. We use incomplete Cholesky's factorization on that purpose. Once H is known, the velocity $V=(u,v,w)$ is finally computed from (2) at the centroids of the interfaces:

$$\begin{aligned} u_{i+\frac{1}{2},j,k} &= -K_{i+\frac{1}{2},j,k}\frac{H_{i+1,j,k}-H_{i,j,k}}{\Delta x_{i+\frac{1}{2}}}, \quad v_{i,j+\frac{1}{2},k} = -K_{i,j+\frac{1}{2},k}\frac{H_{i,j+1,k}-H_{i,j,k}}{\Delta y_{j+\frac{1}{2}}} \\ w_{i,j,k+\frac{1}{2}} &= -K_{i,j,k+\frac{1}{2}}\frac{H_{i,j,k+1}-H_{i,j,k}}{\Delta z_{k+\frac{1}{2}}} \end{aligned} \tag{9}$$

Notice that the velocity satisfies the discrete free-divergence property:

$$\frac{u_{i+\frac{1}{2},j,k}-u_{i-\frac{1}{2},j,k}}{\Delta x_i}+\frac{v_{i,j+\frac{1}{2},k}-v_{i,j-\frac{1}{2},k}}{\Delta y_j}+\frac{w_{i,j,k+\frac{1}{2}}-w_{i,j,k-\frac{1}{2}}}{\Delta z_k}=0 \tag{10}$$

4.2. *Discretization of the transport equation* (5)

The results obtained in this paragraph are justified in Appendix A. First, a first-order accurate numerical scheme approximating (5) is obtained by solving approximate Riemann problems on each interface of a cell (see Appendix A):

$$\begin{aligned} \omega_{i,j,k}c^{n+1}_{i,j,k} = {} & \omega_{i,j,k}c^{n}_{i,j,k} \\ & -\frac{\Delta t}{\Delta x_i}(u^{+}_{i+\frac{1}{2},j,k}c^{n}_{i,j,k}+u^{-}_{i+\frac{1}{2},j,k}c^{n}_{i+1,j,k}-u^{+}_{i-\frac{1}{2},j,k}c^{n}_{i-1,j,k}-u^{-}_{i-\frac{1}{2},j,k}c^{n}_{i,j,k}) \\ & -\frac{\Delta t}{\Delta y_j}(v^{+}_{i,j+\frac{1}{2},k}c^{n}_{i,j,k}+v^{-}_{i,j+\frac{1}{2},k}c^{n}_{i,j+1,k}-v^{+}_{i,j-\frac{1}{2},k}c^{n}_{i,j-1,k}-v^{-}_{i,j-\frac{1}{2},k}c^{n}_{i,j,k}) \\ & -\frac{\Delta t}{\Delta z_k}(w^{+}_{i,j,k+\frac{1}{2}}c^{n}_{i,j,k}+w^{-}_{i,j,k+\frac{1}{2}}c^{n}_{i,j,k+1}-w^{+}_{i,j,k-\frac{1}{2}}c^{n}_{i,j,k-1}-w^{-}_{i,j,k-\frac{1}{2}}c^{n}_{i,j,k}) \\ := {} & \mathscr{M}_{i,j,k} \end{aligned} \tag{11}$$

This scheme is conservative, first-order accurate, l^{∞}-stable and positivity preserving under the CFL condition

$$\frac{\Delta t}{\omega_{i,j,k}}\left(\frac{u^{-}_{i+\frac{1}{2},j,k}+u^{+}_{i-\frac{1}{2},j,k}}{\Delta x_i}+\frac{v^{-}_{i,j+\frac{1}{2},k}+v^{+}_{i,j-\frac{1}{2},k}}{\Delta y_j}+\frac{w^{-}_{i,j,k+\frac{1}{2}}+w^{+}_{i,j,k-\frac{1}{2}}}{\Delta z_k}\right)\leqslant\eta \tag{12}$$

DOI: 10.1002/fld

with $\eta=1$ for all i, j, k. Then, we reduce the spurious numerical diffusion by adding antidiffusion terms in each direction. Setting

$$\Delta c_{i+\frac{1}{2},j,k}:=c_{i+\frac{1}{2},j,k}-c_{i,j,k},\ \Delta c_{i,j+\frac{1}{2},k}:=c_{i,j+\frac{1}{2},k}-c_{i,j,k},\ \Delta c_{i,j,k+\frac{1}{2}}:=c_{i,j,k+\frac{1}{2}}-c_{i,j,k}$$

$$\alpha^{+}_{i+\frac{1}{2},j,k}=u^{+}_{i+\frac{1}{2},j,k}\left(1-\frac{\Delta t u^{+}_{i+\frac{1}{2},j,k}}{\omega_{i+\frac{1}{2},j,k}\Delta x_i}\right),\quad \alpha^{-}_{i+\frac{1}{2},j,k}=u^{-}_{i+\frac{1}{2},j,k}\left(1-\frac{\Delta t u^{-}_{i+\frac{1}{2},j,k}}{\omega_{i+\frac{1}{2},j,k}\Delta x_{i+1}}\right)$$

$$\alpha^{+}_{i,j+\frac{1}{2},k}=v^{+}_{i,j+\frac{1}{2},k}\left(1-\frac{\Delta t v^{+}_{i,j+\frac{1}{2},k}}{\omega_{i,j+\frac{1}{2},k}\Delta y_j}\right),\quad \alpha^{-}_{i,j+\frac{1}{2},k}=v^{-}_{i,j+\frac{1}{2},k}\left(1-\frac{\Delta t v^{-}_{i,j+\frac{1}{2},k}}{\omega_{i,j+\frac{1}{2},k}\Delta y_{j+1}}\right)$$

$$\alpha^{+}_{i,j,k+\frac{1}{2}}=w^{+}_{i,j,k+\frac{1}{2}}\left(1-\frac{\Delta t w^{+}_{i,j,k+\frac{1}{2}}}{\omega_{i,j,k+\frac{1}{2}}\Delta z_k}\right),\quad \alpha^{-}_{i,j,k+\frac{1}{2}}=w^{-}_{i,j,k+\frac{1}{2}}\left(1-\frac{\Delta t w^{-}_{i,j,k+\frac{1}{2}}}{\omega_{i,j,k+\frac{1}{2}}\Delta z_{k+1}}\right)$$

$$r^{+}_{i+\frac{1}{2},j,k}=\frac{u^{+}_{i-\frac{1}{2},j,k}\Delta c_{i-\frac{1}{2},j,k}}{u^{+}_{i+\frac{1}{2},j,k}\Delta c_{i+\frac{1}{2},j,k}},\quad r^{-}_{i-\frac{1}{2}}=\frac{u^{-}_{i+\frac{1}{2},j,k}\Delta c_{i+\frac{1}{2},j,k}}{u^{-}_{i-\frac{1}{2},j,k}\Delta c_{i-\frac{1}{2},j,k}},\quad r^{+}_{i,j+\frac{1}{2},k}=\frac{v^{+}_{i,j-\frac{1}{2},k}\Delta c_{i,j-\frac{1}{2},k}}{v^{+}_{i,j-\frac{1}{2},k}\Delta c_{i,j+\frac{1}{2},k}}$$

$$r^{-}_{i,j-\frac{1}{2},k}=\frac{v^{-}_{i,j+\frac{1}{2},k}\Delta c_{i,j+\frac{1}{2},k}}{v^{-}_{i,j-\frac{1}{2},k}\Delta c_{i,j-\frac{1}{2},k}},\quad r^{+}_{i,j,k+\frac{1}{2}}=\frac{w^{+}_{i,j,k-\frac{1}{2}}\Delta c_{i,j,k-\frac{1}{2}}}{w^{+}_{i,j,k+\frac{1}{2}}\Delta c_{i,j,k+\frac{1}{2}}},\quad r^{-}_{i,j,k-\frac{1}{2}}=\frac{w^{-}_{i,j,k+\frac{1}{2}}\Delta c_{i,j,k+\frac{1}{2}}}{w^{-}_{i,j,k-\frac{1}{2}}\Delta c_{i,j,k-\frac{1}{2}}}$$

$$\phi^{x+}_{i+\frac{1}{2},j,k}=\varphi\left(r^{+}_{i+\frac{1}{2},j,k},\frac{\Delta x_{i+\frac{1}{2}}}{\Delta x_i}\right),\quad \phi^{x-}_{i+\frac{1}{2},j,k}=\varphi\left(r^{-}_{i+\frac{1}{2},j,k},\frac{\Delta x_{i+\frac{1}{2}}}{\Delta x_{i+1}}\right)$$

$$\phi^{y+}_{i,j+\frac{1}{2},k}=\varphi\left(r^{+}_{i,j+\frac{1}{2},k},\frac{\Delta y_{j+\frac{1}{2}}}{\Delta y_j}\right)$$

$$\phi^{y-}_{i,j+\frac{1}{2},k}=\varphi\left(r^{-}_{i,j+\frac{1}{2},k},\frac{\Delta y_{j+\frac{1}{2}}}{\Delta y_{j+1}}\right),\quad \phi^{z+}_{i,j,k+\frac{1}{2}}=\varphi\left(r^{+}_{i,j,k+\frac{1}{2}},\frac{\Delta z_{k+\frac{1}{2}}}{\Delta z_k}\right)$$

$$\phi^{z-}_{i,j,k+\frac{1}{2}}=\varphi\left(r^{-}_{i,j,k+\frac{1}{2}},\frac{\Delta z_{k+\frac{1}{2}}}{\Delta z_{k+1}}\right)$$

where φ is a function satisfying $0\leqslant\varphi(a,b)\leqslant 2b\max(0,\min(1,a))$ for all $(a,b)\in\mathbb{R}\times\mathbb{R}_+$, our advection scheme $\mathscr{S}_1$ is defined by

$$\omega_{i,j,k}c^{n+1}_{i,j,k}=\mathscr{M}_{i,j,k}$$
$$+\frac{1}{2}\frac{\Delta t}{\Delta x_i}\left(\alpha^{-}_{i+\frac{1}{2},j,k}\phi^{x-}_{i+\frac{1}{2},j,k}\Delta c_{i+\frac{1}{2},j,k}\frac{\Delta x_{i+1}}{\Delta x_{i+\frac{1}{2}}}-\alpha^{-}_{i-\frac{1}{2},j,k}\phi^{x-}_{i-\frac{1}{2},j,k}\Delta c_{i-\frac{1}{2},j,k}\frac{\Delta x_i}{\Delta x_{i-\frac{1}{2}}}\right.$$

DOI: 10.1002/fld

$$+\alpha^{+}_{i-\frac{1}{2},j,k}\phi^{x+}_{i-\frac{1}{2},j,k}\Delta c_{i-\frac{1}{2},j,k}\frac{\Delta x_{i-1}}{\Delta x_{i-\frac{1}{2}}}-\alpha^{+}_{i+\frac{1}{2},j,k}\phi^{x+}_{i+\frac{1}{2},j,k}\Delta c_{i+\frac{1}{2},j,k}\frac{\Delta x_i}{\Delta x_{i+\frac{1}{2}}}\Bigg)$$

$$+\frac{1}{2}\frac{\Delta t}{\Delta y_j}\Bigg(\alpha^{-}_{i,j+\frac{1}{2},k}\phi^{y-}_{i,j+\frac{1}{2},k}\Delta c_{i,j+\frac{1}{2},k}\frac{\Delta y_{j+1}}{\Delta y_{j+\frac{1}{2}}}-\alpha^{-}_{i,j-\frac{1}{2},k}\phi^{y-}_{i,j-\frac{1}{2},k}\Delta c_{i,j-\frac{1}{2},k}\frac{\Delta y_j}{\Delta y_{j-\frac{1}{2}}}$$

$$+\alpha^{+}_{i,j-\frac{1}{2},k}\phi^{y+}_{i,j-\frac{1}{2},k}\Delta c_{i,j-\frac{1}{2},k}\frac{\Delta y_{j-1}}{\Delta y_{j-\frac{1}{2}}}-\alpha^{+}_{i,j+\frac{1}{2},k}\phi^{y+}_{i,j+\frac{1}{2},k}\Delta c_{i,j+\frac{1}{2},k}\frac{\Delta y_j}{\Delta y_{j+\frac{1}{2}}}\Bigg)$$

$$+\frac{1}{2}\frac{\Delta t}{\Delta z_k}\Bigg(\alpha^{-}_{i,j,k+\frac{1}{2}}\phi^{z-}_{i,j,k+\frac{1}{2}}\Delta c_{i,j,k+\frac{1}{2}}\frac{\Delta z_{k+1}}{\Delta z_{k+\frac{1}{2}}}-\alpha^{-}_{i,j,k-\frac{1}{2}}\phi^{z-}_{i,j,k-\frac{1}{2}}\Delta c_{i,j,k-\frac{1}{2}}\frac{\Delta z_k}{\Delta z_{k-\frac{1}{2}}}$$

$$+\alpha^{+}_{i,j,k-\frac{1}{2}}\phi^{z+}_{i,j,k-\frac{1}{2}}\Delta c_{i,j,k-\frac{1}{2}}\frac{\Delta z_{k-1}}{\Delta z_{k-\frac{1}{2}}}-\alpha^{+}_{i,j,k+\frac{1}{2}}\phi^{z+}_{i,j,k+\frac{1}{2}}\Delta c_{i,j,k+\frac{1}{2}}\frac{\Delta z_k}{\Delta z_{k+\frac{1}{2}}}\Bigg) \tag{13}$$

This conservative scheme, (13), is l^{∞}-stable and positivity preserving if

$$\Delta t\left(\frac{|u_{i+\frac{1}{2},j,k}|}{\omega_{i+\frac{1}{2},j,k}\min(\Delta x_i,\Delta x_{i+1})},\frac{|v_{i,j+\frac{1}{2},k}|}{\omega_{i,j+\frac{1}{2},k}\min(\Delta y_j,\Delta y_{j+1})},\frac{|w_{i,j,k+\frac{1}{2}}|}{\omega_{i,j,k+\frac{1}{2}}\min(\Delta z_k,\Delta z_{k+1})}\right)\leqslant 1 \tag{14}$$

for all i, j, k, and (12) holds with

$$\eta=\begin{cases}1 & \text{if } B>A^2\\ \dfrac{A+\sqrt{A^2-B}}{B} & \text{otherwise}\end{cases} \tag{15}$$

A simpler (but more restrictive) way of implementing (12) in this case is to select $\eta=\frac{1}{2}$ instead of (15), see Appendix A.

In the following, the function φ is derived from the Superbee limiter [11] and writes:

$$\varphi(a,b)=2b\max(0,\min(1,2a),\min(a,2))$$

Spiral velocity advection test. Our numerical scheme is tested against an academic problem. We let Ω be the unit cube $(0,1)\times(0,1)\times(0,1)$, meshed with the nonuniform grid in Figure 2. The initial condition is discontinuous: its value is 1 inside the ball with center $(0.3, 0.5, 0.15)$ and radius 0.1, and 0 everywhere else. The velocity field is spiral: $V(x,y,z)=(-2\pi(y-\frac{1}{2}),2\pi(x-\frac{1}{2}),0.65)$. The exact solution of this problem remains constant on the spiral characteristic lines imposed by the velocity field. Notice that the transported ball passes through the parallelepiped $(0.2,0.5)\times(0.2,0.4)\times(0.3,0.4)$ where the mesh is refined. This test is reputedly hard because it propagates a discontinuous front. To account for the use of numerical anti-diffusion, we compare the exact solution and the numerical solutions obtained with the first-order Murman scheme (11) and the limited scheme (13) after one revolution (at $t=1$). The exact solution is 1 inside the ball

$$\mathscr{B}=\{(x,y,z),\ (x-0.3)^2+(y-0.5)^2+(z-0.8)^2\geqslant 0.1^2\}$$

DOI: 10.1002/fld

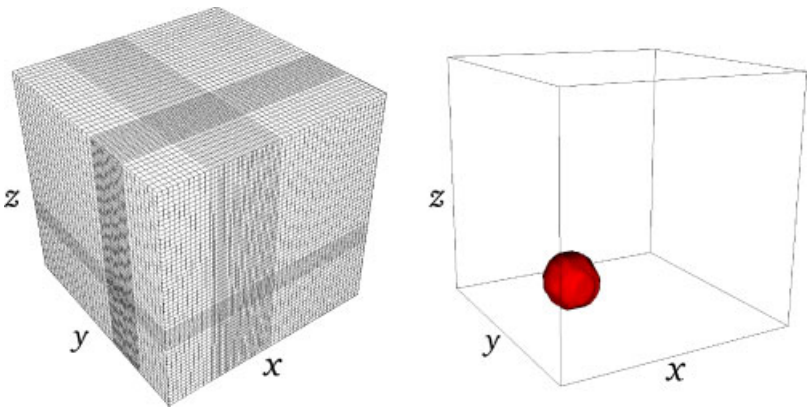

Figure 2. Mesh ($65 \times 47 \times 50$ elements, left) and initial condition (right) for the spiral velocity advection test case.

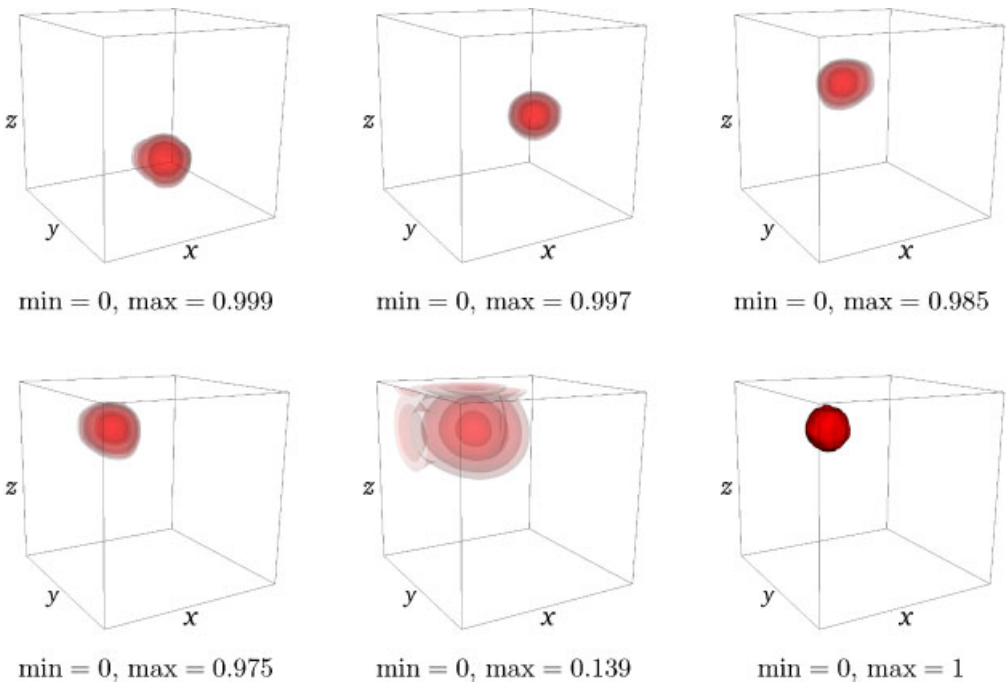

Figure 3. Spiral velocity advection test: Top: from left to right, numerical solution computed with the limited scheme (13) at times $t = 0.25$, $t = 0.5$ and $t = 0.75$. Bottom: from left to right, numerical solution computed with the limited scheme (13), Murman scheme (11), and exact solution at time $t = 1$. The contour values are 0.01, 0.02, 0.05, 0.1, 0.5, 0.7.

and 0 elsewhere. In Figure 3, both numerical schemes offer stable and component-wise nonnegative concentrations. When using the first-order Murman scheme (11), the numerical diffusion is so strong that the numerical solution barely approximates the exact solution. However, our limitation

DOI: 10.1002/fld

Table I. L^1–error and numerical diffusion obtained from the Murman (11) and Limited (13) schemes.

	L^1–error: $\|C_h(1,.)-C(1,.)\|_{L^1(\Omega)}$		Numerical diffusion: $\int_{\Omega\setminus\mathscr{B}} C_h(1,X)\,\mathrm{d}X$	
	Murman scheme	Limited scheme	Murman scheme	Limited scheme
$s=1$ 22 272 cells	8.087×10^{-3}	5.284×10^{-3}	3.944×10^{-3}	2.552×10^{-3}
$s=1/2$ 178 176 cells	7.417×10^{-3}	2.414×10^{-3}	3.731×10^{-3}	1.230×10^{-3}
$s=1/4$ 1 425 408 cells	6.503×10^{-3}	1.204×10^{-3}	3.247×10^{-3}	5.976×10^{-4}
$s=1/8$ 11 403 264 cells	5.236×10^{-3}	6.752×10^{-4}	2.617×10^{-3}	3.368×10^{-4}

technique drastically cuts down the numerical diffusion, though no anti-diffusion is used in the cross directions. As an outcome, the maximum value 1 of the numerical solution obtained from (13) after one turn (at $t=1$) is almost exactly preserved.

Let us denote C_h as the piecewise constant function whose value is C_i^n on each cell Q_i and time interval $[t_n, t_{n+1}[$. In Table I, we report the L^1–error at $t=1$, $\|C_h(1,.)-C(1,.)\|_{L^1(\Omega)}$ and the numerical diffusion, that we define by the mass outside of the theoretical support, $\mathscr{B}$, $\int_{\Omega\setminus\mathscr{B}} C_h(1,X)\,\mathrm{d}X$. Four different meshes are used: the coarsest grid has 22 272 mesh elements and nonconstant mesh-sizes $(\Delta x_i, \Delta y_j, \Delta z_k)_{i,j,k}$. We refine this coarse mesh recursively by using a constant ratio, s, to obtain the three other grids with mesh-sizes $(s\Delta x_i, s\Delta y_j, s\Delta z_k)_{i,j,k}$, for $s=\frac{1}{2},\frac{1}{4},\frac{1}{8}$. The mesh in Figure 2 corresponds with $s=\frac{1}{2}$.

These results quantitatively exhibit that our limitation procedure reduces the numerical diffusion and L^1–error. Figure 4 shows a 0.2th order L^1–convergence for the Murman scheme (11) and a 0.99th order L^1–convergence for the Limited scheme (13), hence illustrating the better accuracy of the latter. Note that since the exact solution is discontinuous, the order of convergence cannot be greater than 1 with any numerical scheme.

4.3. Discretization of the reaction-diffusion equation (6)

In this section, we develop a finite volume numerical scheme approximating (6). Equation (6) is semi-discretized in time by using implicit Euler's scheme:

$$\omega(X)\frac{c(t_{n+1},X)-c(t_n,X)}{\Delta t}-\mathrm{div}(D(X,V(X))\nabla c(t_{n+1},X))$$
$$+\lambda\omega(X)c(t_{n+1},X)=f(t_{n+1},X)+\mathscr{O}(\Delta t)$$

Integrating this equation over any cell $Q_{i,j,k}$ along with using Stokes' formula, we obtain the numerical scheme

$$\omega_{i,j,k}(1+\lambda\Delta t)c_{i,j,k}^{n+1}-\frac{\Delta t}{\Delta x_i\Delta y_j\Delta z_k}\mathscr{L}_{i,j,k}c^{n+1}=\omega_{i,j,k}c_{i,j,k}^{n}+\Delta t f_{i,j,k}^{n+1} \tag{16}$$

DOI: 10.1002/fld

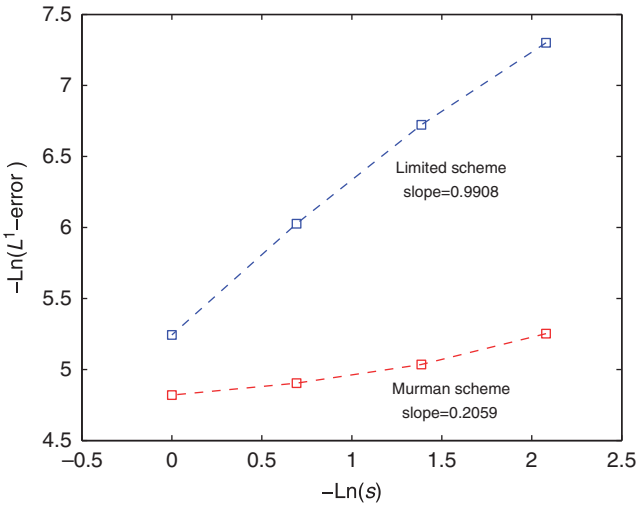

Figure 4. The order of L^1-convergence for the Murman (11) and limited scheme (13) is the slope of the line plotting $-\mathrm{Ln}(\|C_h(1,.)-C(1,.)\|_{L^1(\Omega)})$ versus $-\mathrm{Ln}(s)$.

where the discrete divergence operator

$$\mathscr{L}_{i,j,k}c^{n+1} := F_{i+\frac{1}{2},j,k} - F_{i-\frac{1}{2},j,k} + F_{i,j+\frac{1}{2},k} - F_{i,j-\frac{1}{2},k} + F_{i,j,k+\frac{1}{2}} - F_{i,j,k-\frac{1}{2}}$$

is the sum of the numerical diffusive fluxes across the interfaces:

$$F_{\alpha,\beta,\gamma} \approx \int_{\Gamma_{\alpha,\beta,\gamma}} D(X, V(X))\nabla c(t_{n+1}, X)\cdot \mathbf{v}_{\alpha,\beta,\gamma}\,\mathrm{d}\Gamma$$

for $\alpha = i, i\pm\frac{1}{2}$, $\beta = j, j\pm\frac{1}{2}$, $\gamma = k, k\pm\frac{1}{2}$. Notice that the tensor D is symmetric but not diagonal. We decide to evaluate the diagonal terms $D^{1,1}$, $D^{2,2}$ and $D^{3,3}$ at the centroids $(x_{i\pm\frac{1}{2}}, y_j, z_k)$, $(x_i, y_{j\pm\frac{1}{2}}, z_k)$, $(x_i, y_j, z_{k\pm\frac{1}{2}})$ of the interfaces. The nondiagonal terms $D^{1,2}$, $D^{1,3}$ and $D^{2,3}$ are evaluated on the edges of the interfaces, a 3D counterpart of Reference [3]. The derivatives of $c(t_{n+1}, X)$ are approximated by centered finite difference formulas. Our numerical fluxes in the x-direction are then defined by:

$$\begin{aligned} F_{i+\frac{1}{2},j,k} = \Delta y_j \Delta z_k \Bigg(& D^{1,1}_{i+\frac{1}{2},j,k} \frac{c^{n+1}_{i+1,j,k} - c^{n+1}_{i,j,k}}{\Delta x_{i+\frac{1}{2}}} \\ & + \frac{1}{2}\left(D^{1,2}_{i+\frac{1}{2},j+\frac{1}{2},k} \frac{c^{n+1}_{i+\frac{1}{2},j+\frac{1}{2},k} - c^{n+1}_{i+\frac{1}{2},j,k}}{\Delta y_{j+\frac{1}{2}}} + D^{1,2}_{i+\frac{1}{2},j-\frac{1}{2},k} \frac{c^{n+1}_{i+\frac{1}{2},j,k} - c^{n+1}_{i+\frac{1}{2},j-\frac{1}{2},k}}{\Delta y_{j-\frac{1}{2}}} \right) \\ & + \frac{1}{2}\left(D^{1,3}_{i+\frac{1}{2},j,k+\frac{1}{2}} \frac{c^{n+1}_{i+\frac{1}{2},j,k+\frac{1}{2}} - c^{n+1}_{i+\frac{1}{2},j,k}}{\Delta z_{k+\frac{1}{2}}} + D^{1,2}_{i+\frac{1}{2},j,k-\frac{1}{2}} \frac{c^{n+1}_{i+\frac{1}{2},j,k} - c^{n+1}_{i+\frac{1}{2},j,k-\frac{1}{2}}}{\Delta z_{k-\frac{1}{2}}} \right) \Bigg) \end{aligned}$$

DOI: 10.1002/fld

The fluxes in the other directions, $F_{i,j+\frac{1}{2},k}$ and $F_{i,j,k+\frac{1}{2}}$, are defined in the same fashion. Inside the domain, the concentrations at the interfaces are linearly interpolated from their values at the meshpoints, for instance,

$$\begin{aligned} c^{n+1}_{i+\frac{1}{2},j,k} &= c^{n+1}_{i,j,k} + \frac{1}{2}\frac{\Delta x_i}{\Delta x_{i+\frac{1}{2}}}(c^{n+1}_{i+1,j,k} - c^{n+1}_{i,j,k}) \\ c^{n+1}_{i+\frac{1}{2},j+\frac{1}{2},k} &= c^{n+1}_{i+\frac{1}{2},j,k} + \frac{1}{2}\frac{\Delta y_j}{\Delta y_{j+\frac{1}{2}}}(c^{n+1}_{i+\frac{1}{2},j+1,k} - c^{n+1}_{i+\frac{1}{2},j,k}) \end{aligned} \tag{17}$$

Then, to calculate the terms $D^{1,2}_{i\pm\frac{1}{2},j\pm\frac{1}{2},k}$, $D^{1,3}_{i\pm\frac{1}{2},j,k\pm\frac{1}{2}}$ and $D^{2,3}_{i,j\pm\frac{1}{2},k\pm\frac{1}{2}}$, the values of the geological coefficients α_l, α_t and d_m are evaluated at the interfaces with the same interpolation procedure as the concentrations in (17) from their values at the meshpoints. The velocities at the edges of the interfaces are interpolated from their values obtained by the numerical scheme (9). For example, the velocity in the x-direction is interpolated as

$$u_{i+\frac{1}{2},j+\frac{1}{2},k} = u_{i+\frac{1}{2},j,k} + \frac{1}{2}\frac{\Delta y_j}{\Delta y_{j+\frac{1}{2}}}(u_{i+\frac{1}{2},j+1,k} - u_{i+\frac{1}{2},j,k})$$

$$u_{i+\frac{1}{2},j,k+\frac{1}{2}} = u_{i+\frac{1}{2},j,k} + \frac{1}{2}\frac{\Delta y_j}{\Delta y_{j+\frac{1}{2}}}(u_{i+\frac{1}{2},j,k+1} - w_{i+\frac{1}{2},j,k})$$

$$u_{i,,j+\frac{1}{2},k} = \tfrac{1}{2}(u_{i+\frac{1}{2},j+\frac{1}{2},k} + u_{i-\frac{1}{2},j+\frac{1}{2},k}), \quad u_{i,,j,k+\frac{1}{2}} = \tfrac{1}{2}(u_{i+\frac{1}{2},j,k+\frac{1}{2}} + u_{i-\frac{1}{2},j,k-\frac{1}{2}})$$

After multiplying the implicit scheme (16) by $\Delta x_i \Delta y_j \Delta z_k$, a linear system is to be solved, the matrix of which is symmetric 19-diagonal. With realistic data, the term $\omega/\Delta t$ often dominates the cross terms containing $D^{1,2}$, $D^{1,3}$, $D^{2,3}$ when using the CFL condition (12), (14); this makes the matrix strongly diagonal dominant and the present scheme nonnegativity preserving (see for example [12] and its references) in the applications.

The gradient method is used to inverse this system that is improved by incomplete Choleski pre-conditioning procedure.

5. APPLICATION: THE 3D COUPLEX TEST-CASE

In this section we perform a 3D extension of the well-known 2D Couplex 1 benchmark, *cf.* [2, 13–18]. The goal of this test is to simulate the underground displacement of radioactive Iodine ^{129}I coming from a leak in a nuclear waste repository that lies in a clay layer. This clay layer is surrounded by two limestone layers (from Oxfordian and Dogger era), while a Marl layer represents the near ground on the top of the domain, see Figure 5.

The domain of simulation is the parallelepiped $\Omega = (0, 25\,000\,\mathrm{m}) \times (0, 25\,000\,\mathrm{m}) \times (0, 695\,\mathrm{m})$, which is split into four subdomains:

- The Dogger subdomain is the set $\{(x, y, z) \in \Omega, 0 \leqslant z \leqslant 200\}$.
- The clay subdomain is $\{(x, y, z) \in \Omega, 200 \leqslant z \leqslant \frac{55}{25000}(x + y) + 295\}$.

DOI: 10.1002/fld

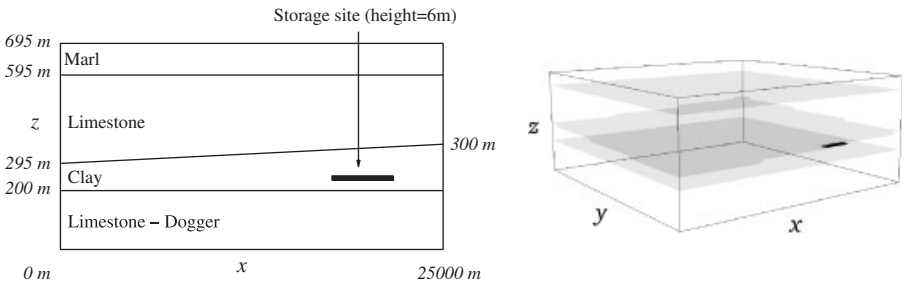

Figure 5. Domain for the 3D couplex test (right) and front face of the domain (left).

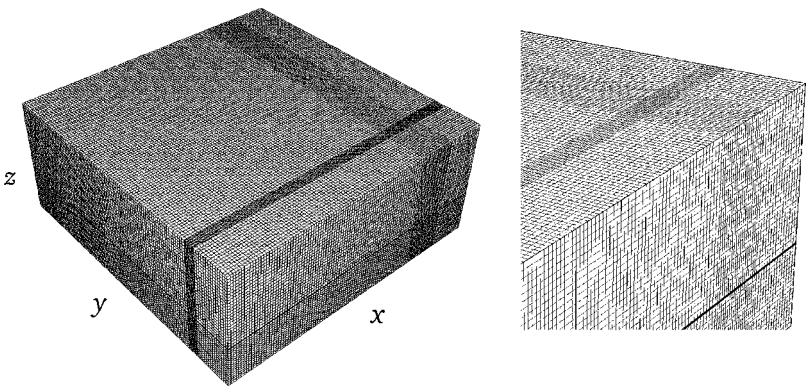

Figure 6. Mesh for the 3D Couplex benchmark: 236 250 elements. Whole domain (left), zoom of the top-right-front region (right).

- The limestone subdomain is $\{(x, y, z) \in \Omega, \frac{55}{25000}(x+y)+295 \leqslant z \leqslant 595\}$.
- The marl subdomain is the set $\{(x, y, z) \in \Omega, 595 \leqslant z \leqslant 695\}$.

The repository $\mathscr{R}$ is modeled by the parallelepiped

$$\mathscr{R} = \{(x, y, z) \in [18\,440, 21\,680] \times [3320, 4320] \times [244, 250]\}$$

Notice that the depth of the domain is quite small compared with its length and width. The dimensions of the repository are also very small compared with the whole domain. Consequently, the mesh is refined around the repository to capture the source of contaminant accurately. In our code, the mesh is handled manually: the user has the option to split the length, width and height of the domain into distinct sub-intervals and select how many cells each sub-interval will be partitioned into. This way, we use a very fine mesh on the intervals $\{x \in (18\,440, 21\,680)\}$, $\{y \in (3320, 4320)\}$ and $\{z \in (244, 250)\}$ so that the repository is captured by several mesh elements. In the rest of the domain we let the mesh coarser in order for the computation time to be fast, see Figure 6.

The data set is entirely provided by the benchmark and is realistic, implying that the geological coefficients ω, k, α_l, α_k and d_m are sharply discontinuous (see Table II). The pollution is simulated

DOI: 10.1002/fld

Table II. Geological coefficients.

	ω	K (m/year)	d_m (m^2/year)	α_l (m)	α_t (m)
Dogger	0.1	25.2288	5×10^{-4}	50	1
Clay	0.001	3.1536×10^{-6}	9.48×10^{-7}	0	0
Limestone	0.1	6.3072	5×10^{-4}	50	1
Marl	0.1	3.1536×10^{-5}	5×10^{-4}	0	0

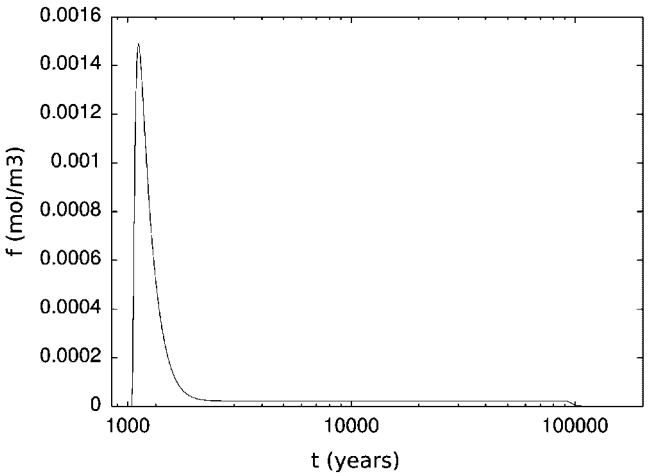

Figure 7. Source term $\bar{f}$ (mol·m^{-3}) versus time (years).

over one million years, while the leak lasts for about a hundred thousand years. The source term f, modeling the leak, vanishes outside the repository and is assumed to be constant in space inside. More precisely, we set

$$f(t,X)=\frac{\bar{f}(t)}{|\mathscr{R}|}\chi_{\mathscr{R}}(X)$$

where $\chi_{\mathscr{R}}$ stands for the characteristic function of the repository $\mathscr{R}$, $|\mathscr{R}|$ is the volume of $\mathscr{R}$, and $\bar{f}$ is a piecewise linear function whose graph is plotted in Figure 7 and values are imposed by the benchmark. The period of the element ^{129}I is $T=1.57\times10^7$ years, and the radioactive decay factor is given by $\lambda=\mathrm{Ln}2/T$.

We assume that there is no contamination at time $t=0$: our initial condition is $c(0,.)\equiv0$ over the whole domain. The boundary conditions are summarized on Table III.

Our numerical result for the hydrodynamic load (expressed in m) and velocity (expressed in m/year) are displayed in Figures 8 and 9. The hydrodynamic load accounts for the pressure on the fluid. Hence, the flow will be directed from the higher loads to the lower loads. The speed

DOI: 10.1002/fld

Table III. Boundary conditions (the symbol 'n.a.' means 'not applicable').

	Dogger	Clay	Limestone	Marl
Bottom boundary ($z=0$)	$D\nabla c\cdot\mathbf{v}-cV\cdot\mathbf{v}=0$ $V\cdot\mathbf{v}=0$	n.a.	n.a.	n.a.
Top boundary ($z=695$)	n.a.	n.a.	n.a.	$c=0$ $H=250+\frac{90}{25000}x-\frac{70}{25000}y$
Left boundary ($x=0$)	$\nabla c\cdot\mathbf{v}=0$ $H=287-\frac{y}{25000}$	$\nabla c\cdot\mathbf{v}=0$ $V\cdot\mathbf{v}=0$	$\nabla c\cdot\mathbf{v}=0$ $H=250-\frac{50}{25000}y$	$\nabla c\cdot\mathbf{v}=0$ $V\cdot\mathbf{v}=0$
Right boundary ($x=25000$)	$\nabla c\cdot\mathbf{v}=0$ $H=289-\frac{2}{25000}y$	$\nabla c\cdot\mathbf{v}=0$ $V\cdot\mathbf{v}=0$	$\nabla c\cdot\mathbf{v}=0$ $H=310-\frac{60}{25000}y$	$\nabla c\cdot\mathbf{v}=0$ $V\cdot\mathbf{v}=0$
Front boundary ($y=0$)	$\nabla c\cdot\mathbf{v}=0$ $H=287+\frac{2}{25000}x$	$\nabla c\cdot\mathbf{v}=0$ $V\cdot\mathbf{v}=0$	$\nabla c\cdot\mathbf{v}=0$ $H=250+\frac{50}{25000}x$	$\nabla c\cdot\mathbf{v}=0$ $V\cdot\mathbf{v}=0$
Back boundary ($y=25000$)	$\nabla c\cdot\mathbf{v}=0$ $H=286+\frac{x}{25000}$	$\nabla c\cdot\mathbf{v}=0$ $V\cdot\mathbf{v}=0$	transparent in c $H=200+\frac{50}{25000}x$	$\nabla c\cdot\mathbf{v}=0$ $V\cdot\mathbf{v}=0$

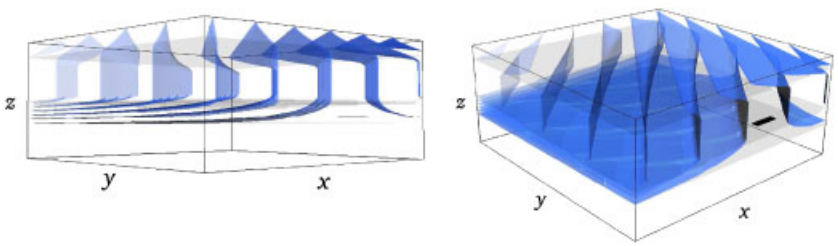

Figure 8. Hydrodynamic load contours for the 3D COUPLEX test case with 10 isovalues between 180 m (light) and 340 m (dark).

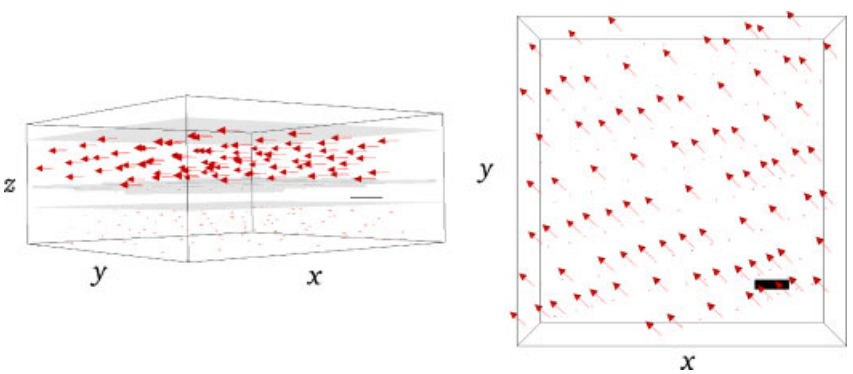

Figure 9. Velocity (m/year) for the 3D COUPLEX test case ($8.11\times10^{-10}\leqslant|V|\leqslant0.022$).

ranges from 8.11×10^{-10} m/year to 0.022 m/year. It is the fastest in the limestone layer, while it is negligible in both clay and Marl layer, as an outcome of very small permeabilities. Our computed concentrations are displayed in Figures 10–14. The convection phenomenon can be observed in

DOI: 10.1002/fld

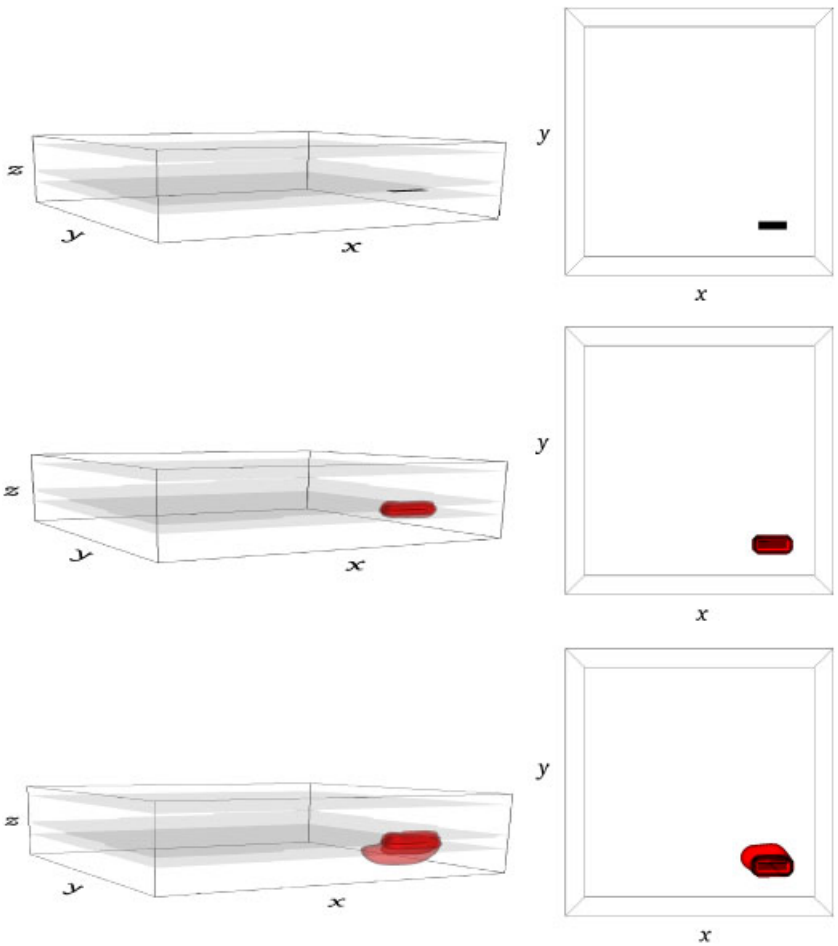

Figure 10. Numerical concentrations of ^{129}I from top to bottom at times $t=0$, $t=10\,110$, $t=70\,000$ years. The left column in an oblique view of the domain and the right column is a view of the domain from the top. The contour values are 10^{-12} (light), 10^{-10} (medium), 10^{-8} (dark) mol/m^3.

the Dogger and limestonelayers, while diffusion is dominant in the clay and Marl layers due to a very small velocity.

First, the pollutant progressively invades the clay layer, in which the permeability and velocity are very weak and avoid advection/dispersion phenomena. After about 10 110 years, the pollutant diffuses out of its storage clay layer to the Dogger layer, see Figure 10. After about 70 000 years, some radio-elements also reach the limestone layer. In Figures 11 and 12, the radioelements progressively invade the underground.

In the limestone and Dogger layers, the molecular diffusion still plays a role. However, the velocity in these layers is significant and most of the motion is then due to advection and mechanical dispersion. Indeed, the invasion progresses the fastest in the limestone layer, where the speed is the highest.

DOI: 10.1002/fld

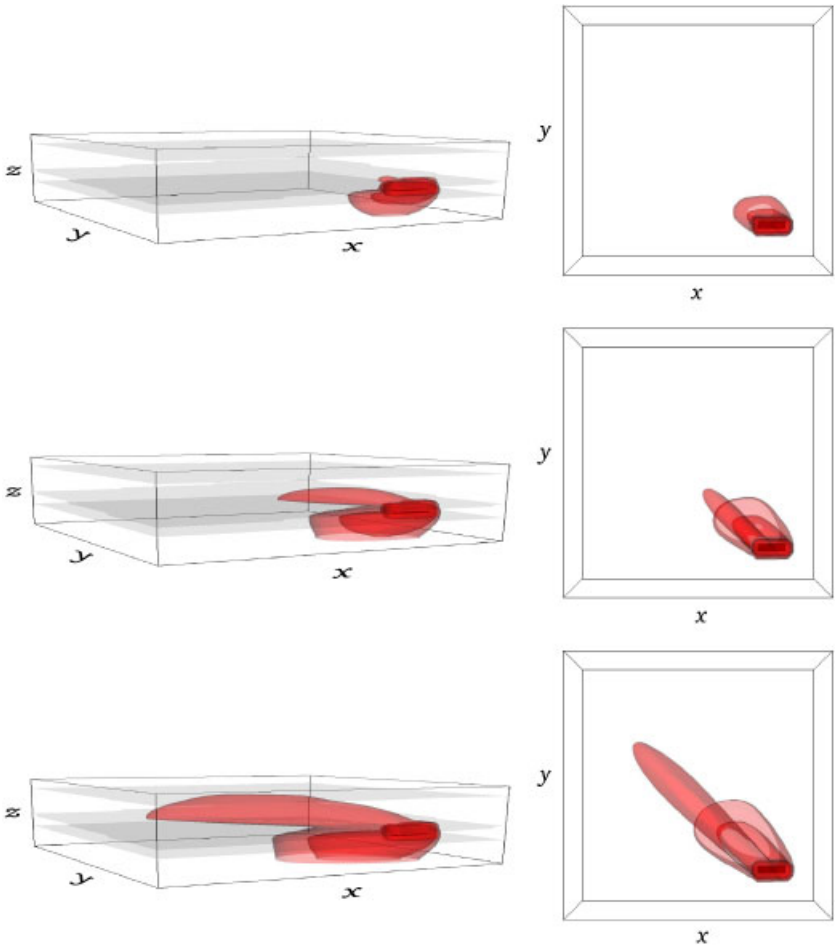

Figure 11. Numerical concentrations of ^{129}I from top to bottom at times $t=100\,000$, $t=200\,000$ and $t=300\,000$. The left column in an oblique view of the domain and the right column is a view of the domain from the top. The contour values are 10^{-12} (light), 10^{-10} (medium), 10^{-8} (dark) mol/m^3.

We can observe that some radionuclides hit the Marl layer after about 500 000 years and eventually reach the surface of the ground. When the source of contaminant is no longer active, the pollution progressively dissapears as the concentrations become too weak to counter the effect of the radioactive decay phenomenon, see Figures 13 and 14. The particles are then destroyed along time as a result of radioactive decay.

The behavior of our 3D numerical solutions matches former 2D results [2, 3] and confirms our expectations: some radionuclides reach the ground surface before being destroyed.

However, our results should be considered more realistic than 2D results, as real grounds are 3D. Indeed, since the top of the clay layer is an inclined plane whose slopes are different in the x-and y-directions, the geometry of the present test case cannot be described by a 2D domain.

DOI: 10.1002/fld

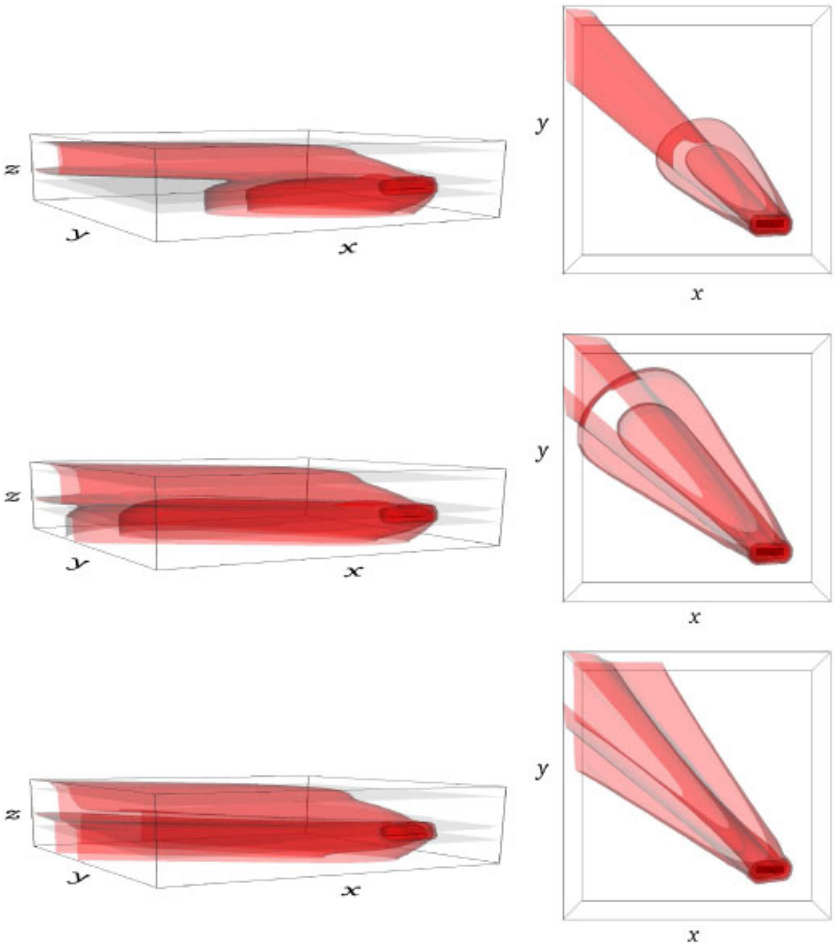

Figure 12. Numerical concentrations of ^{129}I from top to bottom at times $t = 500\,000$, $t = 10^6$ and $t = 2 \times 10^6$ years. The left column in an oblique view of the domain and the right column is a view of the domain from the top. The contour values are 10^{-12} (light), 10^{-10} (medium), 10^{-8} (dark) mol/m^3.

6. COMPUTATIONAL RESOURCES

All the simulations presented in this paper were performed on a MacBookPro machine, featuring a 2.33 GHz intel Core 2 Duo processor with a clock rate of 667 MHz and a total memory of 2000 MBytes.

Indeed, a main concern with 3D simulations is whether the numerical solutions are computed fast enough.

In order to test the performance of our method, we compare the runtimes for the 3D COUPLEX test case over 100 000 years on three different independent grids: grid 1:159, 936 ($68 \times 49 \times 48$) mesh elements, grid 2: 236, 250 ($75 \times 70 \times 45$) mesh elements and grid 3: 1 347,597 ($131 \times 127 \times 81$) mesh elements.

DOI: 10.1002/fld

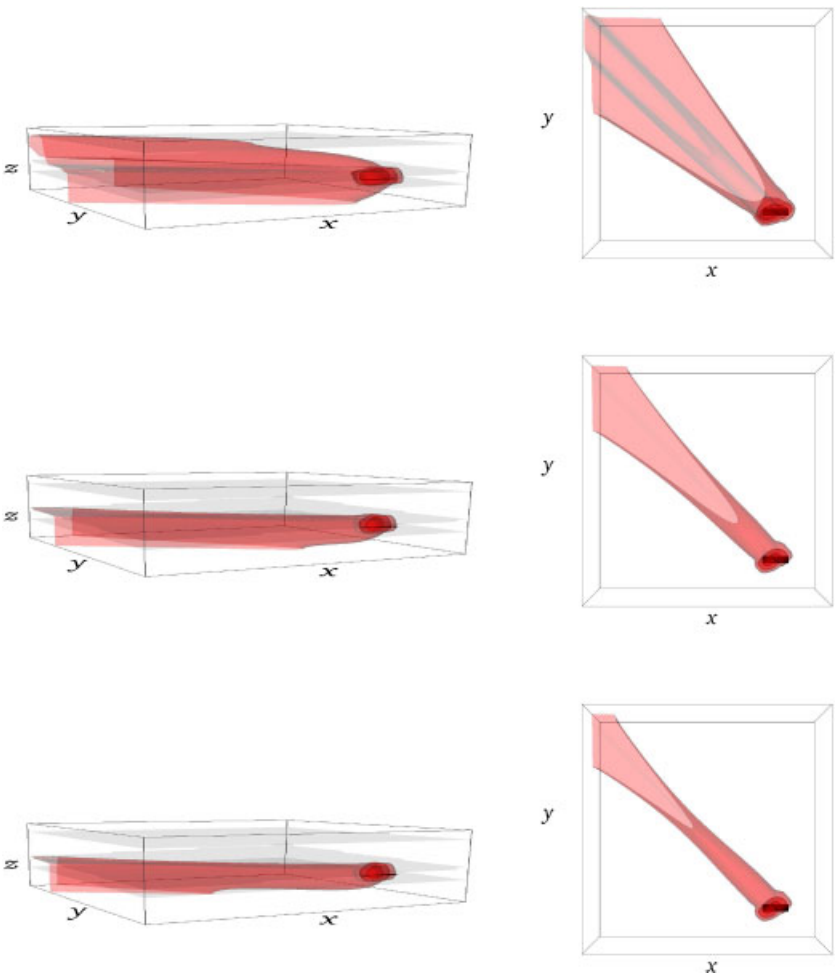

Figure 13. Numerical concentrations of ^{129}I from top to bottom at times $t = 4 \times 10^6$, $t = 7 \times 10^6$ and $7.5 \times t = 10^6$ years. The left column in an oblique view of the domain and the right column is a view of the domain from the top. The contour values are 10^{-12} (light), 10^{-10} (medium), 10^{-8} (dark) mol/m^3.

Table IV shows that our numerical solutions are calculated in a reasonable time. The CPU time per iteration per grid point is almost constant, hence showing that the rate of convergence is independent of time and mesh. Note that the three grids are not related to each other, and grid 2 offers the smallest CFL ratio in the left-hand side of (12). Therefore, it requires the most iterations.

7. CONCLUSION

3D numerical simulations involving heterogeneous data have always been an interesting mathematical and engineering challenge.

DOI: 10.1002/fld

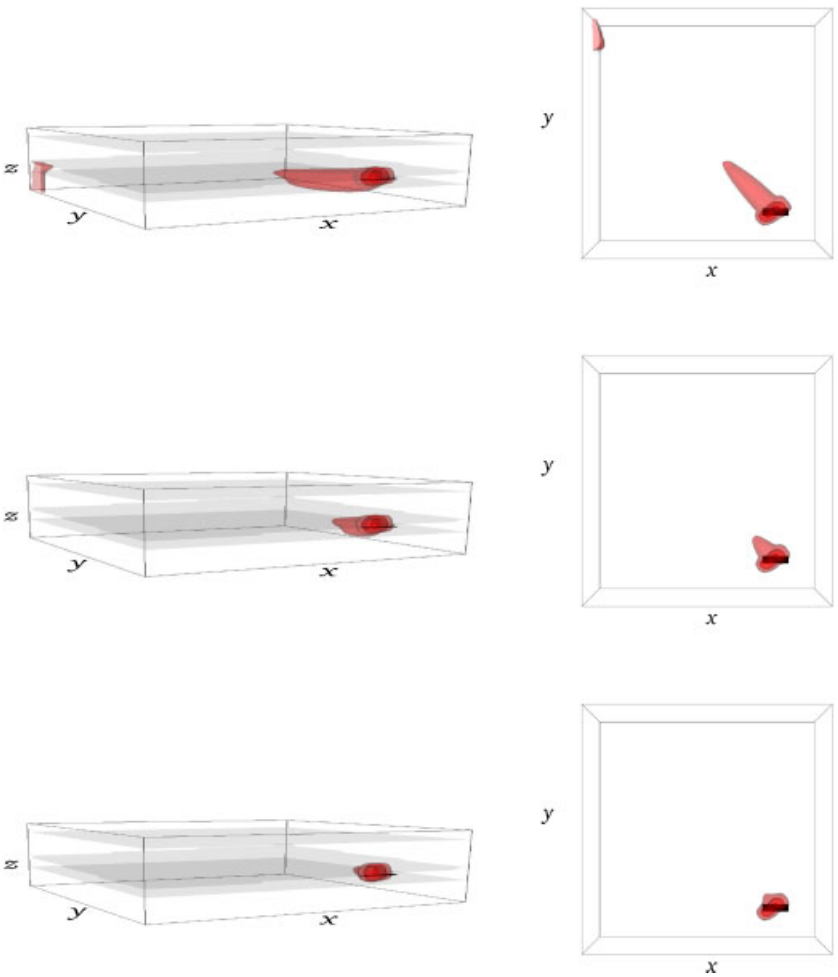

Figure 14. Numerical concentrations of ^{129}I from top to bottom at times $t = 8 \times 10^6$, $t = 9 \times 10^6$ and $t = 10^7$ years. The left column in an oblique view of the domain and the right column is a view of the domain from the top. The contour values are 10^{-12} (light), 10^{-10} (medium), 10^{-8} (dark) mol/m^3.

We have developed an effective method to simulate the radionuclide transport through highly heterogeneous 3D grounds. Indeed, our method makes it possible to handle realistic data, as shown in Section 5.

The use of mesh refinements in each direction enables us to discretize the source term without much impacting the computation time.

Our anti-diffusive technique reduces the spurious numerical diffusion, so the advection operator is discretized accurately. Advection and reaction/diffusion schemes are then plugged into an operator splitting procedure gathering all the phenomena in the model.

For sustainable development concerns, we observed that geological coefficients and pressure conditions can be such that escaped radionuclides reach the ground surface. Therefore, underground

DOI: 10.1002/fld

Table IV. Comparison of CPU time on three grids for a simulation time of 100 000 years.

	Grid 1	Grid 2	Grid 3
Meshes	159 936	259 008	1 347 597
Memory used (MBytes)	74	120	612
Number of iterations	719	1065	797
CPU (s)	1038	2570	10 440
CPU/iteration/grid point	9.02×10^{-6}	9.31×10^{-6}	9.72^{-6}

disposal sites might be unsafe for populations and yield a disaster if not carefully implemented. For this reason, we feel that this paper might be used as an illustration within a politico-social context.

An interesting possible extension to this work is to study whether a change in the data can reduce the threat. Indeed, other pressure conditions would influence the flow through pervious rocks, hence modifying the particle transport pattern. However, the molecular diffusion effect only depends on the nature of the rocks and would remain unchanged. So, we feel that even a suitable flow would not be enough to prevent the radionuclide from reaching the surface. Other alternatives include changing the storage environment and investigating what permeability, storage depth and rocks surrounding the disposal site might yield a safer outcome.

APPENDIX A: CONSTRUCTION OF THE SCHEME (13)

To place matters in perspective, consider Equation (5) in one space dimension, denote x as the independent space variable in a space domain $(0, L_x)$, that is an interval. The meshpoints are denoted by x_i, as defined as in Section 3.1, with steps Δx_i and $\Delta x_{i\pm\frac{1}{2}}$. We construct a numerical scheme from the widely used transport-projection technique (see [3, 19]).

Denoting c_i^n as an approximation of $\frac{1}{\Delta x_i}\int_{x_{i-\frac{1}{2}}}^{x_{i+\frac{1}{2}}} c(t_n,x)\,\mathrm{d}x$, we integrate Equation (5) over one cell $(x_{i-\frac{1}{2}}, x_{i+\frac{1}{2}})$:

$$\Delta x_i\omega_i c_i^{n+1} = \Delta x_i\omega_i c_i^n - \int_{t_n}^{t_{n+1}} u_{i+\frac{1}{2}}c(t,x_{i+\frac{1}{2}}) - u_{i-\frac{1}{2}}c(t,x_{i-\frac{1}{2}})\,\mathrm{d}t \tag{A1}$$

Then, the concentration $c(t,x_{i+\frac{1}{2}})$ at the interface $x_{i+\frac{1}{2}}$ is approximated by $\tilde{c}(t,0)$, where $\tilde{c}$ is the solution to the following exact Riemann problem with constant velocity field:

$$\begin{cases} \partial_t\tilde{c} + \dfrac{u_{i+\frac{1}{2}}}{\omega_{i+\frac{1}{2}}}\partial_x\tilde{c} = 0, \quad (t,x)\in\mathbb{R}_+\times\mathbb{R} \\ \tilde{c}(0,x) = c_i^n, \quad x\in(-\infty,0) \\ \tilde{c}(0,x) = c_{i+1}^n, \quad x\in(0,+\infty) \end{cases} \qquad \text{so } c(t,x_{i+\frac{1}{2}}) = \begin{cases} c_i^n & \text{if } u_{i+\frac{1}{2}}>0 \\ c_{i+1}^n & \text{if } u_{i+\frac{1}{2}}<0 \end{cases}$$

DOI: 10.1002/fld

Repeating this process on the interface $x_{i-\frac{1}{2}}$ and plugging the results into (A1) yield the Murman scheme with nonconstant velocity:

$$\omega_i c_i^{n+1} = \omega_i c_i^n - \frac{\Delta t}{\Delta x_i}(u^+_{i+\frac{1}{2}} c_i^n + u^-_{i+\frac{1}{2}} c_{i+1}^n - u^+_{i-\frac{1}{2}} c_{i-1}^n - u^-_{i-\frac{1}{2}} c_i^n) \tag{A2}$$

To increase the accuracy, we notice that $\partial_t c = -(1/\omega)\partial_x(uc)$ and if c is regular enough,

$$\partial_t^2 c = \frac{1}{\omega}\partial_x\left(\frac{u}{\omega}\partial_x(uc)\right)$$

Therefore, integrating the second degree Taylor polynomial for c with respect to t over one cell leads to:

$$\begin{aligned}\int_{x_{i-\frac{1}{2}}}^{x_{i+\frac{1}{2}}} \omega(x)c(t_{n+1},x)\,\mathrm{d}x = &\int_{x_{i-\frac{1}{2}}}^{x_{i+\frac{1}{2}}} \omega(x)c(t_n,x)\,\mathrm{d}x\\ &-\Delta t\,(u_{i+\frac{1}{2}}c(t_n,x_{i+\frac{1}{2}}) - u_{i-\frac{1}{2}}c(t_n,x_{i-\frac{1}{2}}))\\ &+\frac{\Delta t^2}{2}\left(\frac{u^2_{i+\frac{1}{2}}}{\omega_{i+\frac{1}{2}}}\partial_x c(t_n,x_{i+\frac{1}{2}}) - \frac{u^2_{i-\frac{1}{2}}}{\omega_{i-\frac{1}{2}}}\partial_x c(t_n,x_{i-\frac{1}{2}})\right)\\ &+\frac{\Delta t^2}{2}\left(c(t_n,x_{i+\frac{1}{2}})\frac{u_{i+\frac{1}{2}}}{\omega_{i+\frac{1}{2}}}\partial_x u(x_{i+\frac{1}{2}}) - c(t_n,x_{i-\frac{1}{2}})\frac{u_{i-\frac{1}{2}}}{\omega_{i-\frac{1}{2}}}\partial_x u(x_{i-\frac{1}{2}})\right)\\ &+\mathcal{O}(\Delta t^3)\end{aligned} \tag{A3}$$

Then, $c(t_n, x_{i+\frac{1}{2}})$ is approximated by interpolating c^n linearly on the interface $x_{i+\frac{1}{2}}$ and the derivative of c is discretized centrally:

$$c^n_{i+\frac{1}{2}} = \frac{1}{2}\left(\frac{\Delta x_{i+1}}{\Delta x_{i+\frac{1}{2}}}c_i^n + \frac{\Delta x_i}{\Delta x_{i+\frac{1}{2}}}c_{i+1}^n\right), \quad \partial_x c(t_n, x_{i+\frac{1}{2}}) \approx \frac{c^n_{i+1} - c^n_i}{\Delta x_{i+\frac{1}{2}}}$$

Negliging $\partial_x u$ in (A3) (since in three space dimensions our velocity is divergence free), we obtain the Lax-Wendroff-like numerical scheme:

$$\begin{aligned}\omega_i c_i^{n+1} = \omega_i c_i^n - \frac{\Delta t}{2\Delta x_i}&\left(u_{i+\frac{1}{2}}\left(\frac{\Delta x_{i+1}}{\Delta x_{i+\frac{1}{2}}}c_i^n + \frac{\Delta x_i}{\Delta x_{i+\frac{1}{2}}}c_{i+1}^n\right) - u_{i-\frac{1}{2}}\left(\frac{\Delta x_{i-1}}{\Delta x_{i-\frac{1}{2}}}c_i^n + \frac{\Delta x_i}{\Delta x_{i-\frac{1}{2}}}c_{i-1}^n\right)\right)\\ &+\frac{\Delta t^2}{2\Delta x_i}\left(\frac{u^2_{i+\frac{1}{2}}}{\omega_{i+\frac{1}{2}}}\frac{c_{i+1}-c_i}{\Delta x_{i+\frac{1}{2}}} - \frac{u^2_{i-\frac{1}{2}}}{\omega_{i-\frac{1}{2}}}\frac{c_i - c_{i-1}}{\Delta x_{i-\frac{1}{2}}}\right)\end{aligned} \tag{A4}$$

DOI: 10.1002/fld

In three space dimensions, the scheme (11) is obtained in the same fashion as (A2), by integrating (5) over one cell and solving Riemann problems in each direction x, y, z. That scheme can be rewritten as

$$\begin{aligned}\omega_{i,j,k}c^{n+1}_{i,j,k} = \omega_{i,j,k}c^{n}_{i,j,k} - \mathscr{A}_{i,j,k} &- \frac{\Delta t}{\Delta x_i}\left(u^{-}_{i+\frac{1}{2},j,k}\Delta c^{n}_{i+\frac{1}{2},j,k} + u^{+}_{i-\frac{1}{2},j,k}\Delta c^{n}_{i-\frac{1}{2},j,k}\right)\\ &- \frac{\Delta t}{\Delta y_j}\left(v^{-}_{i,j+\frac{1}{2},k}\Delta c^{n}_{i,j+\frac{1}{2},k} + v^{+}_{i,j-\frac{1}{2},k}\Delta c^{n}_{i,j-\frac{1}{2},k}\right)\\ &- \frac{\Delta t}{\Delta z_k}\left(w^{-}_{i,j,k+\frac{1}{2}}\Delta c^{n}_{i,j,k+\frac{1}{2}} - w^{+}_{i,j,k-\frac{1}{2}}\Delta c^{n}_{i,j,k-\frac{1}{2}}\right)\end{aligned} \tag{A5}$$

where $\Delta c^{n}_{i+\frac{1}{2},j,k}$, $\Delta c^{n}_{i,j+\frac{1}{2},k}$, $\Delta c^{n}_{i,j,k+\frac{1}{2}}$ are defined in Subsection 4.2 and

$$\mathscr{A}_{i,j,k} := \frac{u_{i+\frac{1}{2},j,k} - u_{i-\frac{1}{2},j,k}}{\Delta x_i} + \frac{v_{i,j+\frac{1}{2},k} - v_{i,j-\frac{1}{2},k}}{\Delta y_j} + \frac{w_{i,j,k+\frac{1}{2}} - w_{i,j,k-\frac{1}{2}}}{\Delta z_k} = 0$$

from (10). The right-hand side of (A5) is then a convex combination of the discrete concentrations at time t_n as long as condition (12) holds, implying nonnegativity preservation and stability of the scheme (11).

Then, using the notations

$$c^{n}_{i+\frac{1}{2},j,k} = \frac{1}{2}\left(\frac{\Delta x_{i+1}}{\Delta x_{i+\frac{1}{2}}}c^{n}_{i,j,k} + \frac{\Delta x_i}{\Delta x_{i+\frac{1}{2}}}c^{n}_{i+1,j,k}\right), \quad c^{n}_{i,j+\frac{1}{2},k} = \frac{1}{2}\left(\frac{\Delta y_{j+1}}{\Delta y_{j+\frac{1}{2}}}c^{n}_{i,j,k} + \frac{\Delta y_j}{\Delta y_{j+\frac{1}{2}}}c^{n}_{i,j+1,k}\right)$$

$$c^{n}_{i,j,k+\frac{1}{2}} = \frac{1}{2}\left(\frac{\Delta z_{k+1}}{\Delta z_{k+\frac{1}{2}}}c^{n}_{i,j,k} + \frac{\Delta z_k}{\Delta z_{k+\frac{1}{2}}}c^{n}_{i,j,k+1}\right)$$

our 3D antidiffusive scheme is defined by writing the numerical fluxes of (A4) in each direction:

$$\begin{aligned}\omega_{i,j,k}c^{n+1}_{i,j,k} = \omega_{i,j,k}c^{n}_{i,j,k} - \frac{\Delta t}{\Delta x_i}\Bigg(&u_{i+\frac{1}{2},j,k}c^{n}_{i+\frac{1}{2},j,k} - u_{i-\frac{1}{2},j,k}c^{n}_{i-\frac{1}{2},j,k}\\ &- \frac{\Delta t}{2}\left(\frac{u^2_{i+\frac{1}{2},j,k}}{\omega_{i+\frac{1}{2},j,k}}\frac{\Delta c^{n}_{i+\frac{1}{2},j,k}}{\Delta x_{i+\frac{1}{2}}} - \frac{u^2_{i-\frac{1}{2},j,k}}{\omega_{i-\frac{1}{2},j,k}}\frac{\Delta c^{n}_{i-\frac{1}{2},j,k}}{\Delta x_{i-\frac{1}{2}}}\right)\Bigg)\\ - \frac{\Delta t}{\Delta y_j}\Bigg(&v_{i,j+\frac{1}{2},k}c^{n}_{i,j+\frac{1}{2},k} - v_{i,j-\frac{1}{2},k}c^{n}_{i,j-\frac{1}{2},k}\\ &- \frac{\Delta t}{2}\left(\frac{v^2_{i,j+\frac{1}{2},k}}{\omega_{i,j+\frac{1}{2},k}}\frac{\Delta c^{n}_{i,j+\frac{1}{2},k}}{\Delta y_{j+\frac{1}{2}}} - \frac{v^2_{i,j-\frac{1}{2},k}}{\omega_{i,j-\frac{1}{2},k}}\frac{\Delta c^{n}_{i,j-\frac{1}{2},k}}{\Delta y_{j-\frac{1}{2}}}\right)\Bigg)\end{aligned}$$

DOI: 10.1002/fld

$$-\frac{\Delta t}{\Delta z_k}\left(w_{i,j,k+\frac{1}{2}}c^n_{i,j,k+\frac{1}{2}}-w_{i,j,k-\frac{1}{2}}c^n_{i,j,k-\frac{1}{2}}\right.$$

$$\left.-\frac{\Delta t}{2}\left(\frac{w^2_{i,j,k+\frac{1}{2}}}{\omega_{i,j,k+\frac{1}{2}}}\frac{\Delta c^n_{i,j,k+\frac{1}{2}}}{\Delta z_{k+\frac{1}{2}}}-\frac{w^2_{i,j,k-\frac{1}{2}}}{\omega_{i,j,k-\frac{1}{2}}}\frac{\Delta c^n_{i,j,k-\frac{1}{2}}}{\Delta z_{k-\frac{1}{2}}}\right)\right) \tag{A6}$$

Notice that scheme (13) can be obtained from the second degree Taylor polynomial for c as in (A3), using $\mathrm{div}V=0$ and negliging all the terms in the form $\Delta t^2\partial^2_{ab}c$ with notations $a=x,y,z$, $b=x,y,z$ and $a\neq b$. Hence, this scheme is still first-order accurate. However, it is more accurate than (11). Indeed, our antidiffusion technique cuts down the numerical diffusion considerably, as observed in the spiral velocity test case (Section 4.2).

Finally, we stabilize the numerical scheme (A6) by limiting the antidiffusion terms (we refer, for example, to [3, 19–21] and their references). Scheme (A6) is written as a perturbation of Murman-3D scheme (11):

$$\begin{aligned}
\omega_{i,j,k}c^{n+1}_{i,j,k}=\mathscr{M}_{i,j,k}&+\frac{1}{2}\frac{\Delta t}{\Delta x_i}\left(\alpha^-_{i+\frac{1}{2},j,k}\Delta c_{i+\frac{1}{2},j,k}\frac{\Delta x_{i+1}}{\Delta x_{i+\frac{1}{2}}}-\alpha^-_{i-\frac{1}{2},j,k}\Delta c_{i-\frac{1}{2},j,k}\frac{\Delta x_i}{\Delta x_{i-\frac{1}{2}}}\right.\\
&\left.+\alpha^+_{i-\frac{1}{2},j,k}\Delta c_{i-\frac{1}{2},j,k}\frac{\Delta x_{i-1}}{\Delta x_{i-\frac{1}{2}}}-\alpha^+_{i+\frac{1}{2},j,k}\Delta c_{i+\frac{1}{2},j,k}\frac{\Delta x_i}{\Delta x_{i+\frac{1}{2}}}\right)\\
&+\frac{1}{2}\frac{\Delta t}{\Delta y_j}\left(\alpha^-_{i,j+\frac{1}{2},k}\Delta c_{i,j+\frac{1}{2},k}\frac{\Delta y_{j+1}}{\Delta y_{j+\frac{1}{2}}}-\alpha^-_{i,j-\frac{1}{2},k}\Delta c_{i,j-\frac{1}{2},k}\frac{\Delta y_j}{\Delta y_{j-\frac{1}{2}}}\right.\\
&\left.+\alpha^+_{i,j-\frac{1}{2},k}\Delta c_{i,j-\frac{1}{2},k}\frac{\Delta y_{j-1}}{\Delta y_{j-\frac{1}{2}}}-\alpha^+_{i,j+\frac{1}{2},k}\Delta c_{i,j+\frac{1}{2},k}\frac{\Delta y_j}{\Delta y_{j+\frac{1}{2}}}\right)\\
&+\frac{1}{2}\frac{\Delta t}{\Delta z_k}\left(\alpha^-_{i,j,k+\frac{1}{2}}\Delta c_{i,j,k+\frac{1}{2}}\frac{\Delta z_{k+1}}{\Delta z_{k+\frac{1}{2}}}-\alpha^-_{i,j,k-\frac{1}{2}}\Delta c_{i,j,k-\frac{1}{2}}\frac{\Delta z_k}{\Delta z_{k-\frac{1}{2}}}\right.\\
&\left.+\alpha^+_{i,j,k-\frac{1}{2}}\Delta c_{i,j,k-\frac{1}{2}}\frac{\Delta z_{k-1}}{\Delta z_{k-\frac{1}{2}}}-\alpha^+_{i,j,k+\frac{1}{2}}\Delta c_{i,j,k+\frac{1}{2}}\frac{\Delta z_k}{\Delta z_{k+\frac{1}{2}}}\right)
\end{aligned}$$

Multiplying each anti-diffusion term by an appropriate limiter, we obtain the numerical scheme (13), for which

$$\begin{aligned}
c^{n+1}_{i,j,k}=c^n_{i,j,k}&+A_{i+\frac{1}{2},j,k}\Delta c^n_{i+\frac{1}{2},j,k}-B_{i-\frac{1}{2},j,k}\Delta c^n_{i-\frac{1}{2},j,k}+A_{i,j+\frac{1}{2},k}\Delta c^n_{i,j+\frac{1}{2},k}\\
&-B_{i,j-\frac{1}{2},k}\Delta c^n_{i,j-\frac{1}{2},k}+A_{i,j,k+\frac{1}{2}}\Delta c^n_{i,j,k+\frac{1}{2}}-B_{i,j,k-\frac{1}{2}}\Delta c^n_{i,j,k-\frac{1}{2}}
\end{aligned}$$

DOI: 10.1002/fld

with

$$A_{i+\frac{1}{2},j,k} = -\frac{\Delta t u^{-}_{i+\frac{1}{2},j,k}}{\omega_{i,j,k}\Delta x_i}\left(1-\frac{1}{2}\left(1+\frac{\Delta t u^{-}_{i+\frac{1}{2},j,k}}{\omega_{i+\frac{1}{2},j,k}\Delta x_{i+1}}\right)\frac{\Delta x_{i+1}}{\Delta x_{i+\frac{1}{2}}}\phi^{x-}_{i+\frac{1}{2},j,k}\right.$$
$$\left.+\frac{1}{2}\left(1+\frac{\Delta t u^{-}_{i-\frac{1}{2},j,k}}{\omega_{i-\frac{1}{2},j,k}\Delta x_i}\right)\frac{\Delta x_i}{\Delta x_{i-\frac{1}{2}}}\frac{\phi^{x-}_{i-\frac{1}{2},j,k}}{r^{-}_{i-\frac{1}{2},j,k}}\right)$$

$$B_{i-\frac{1}{2},j,k} = \frac{\Delta t u^{+}_{i-\frac{1}{2},j,k}}{\omega_{i,j,k}\Delta x_i}\left(1-\frac{1}{2}\left(1-\frac{\Delta t u^{+}_{i-\frac{1}{2},j,k}}{\omega_{i-\frac{1}{2},j,k}\Delta x_{i-1}}\right)\frac{\Delta x_{i-1}}{\Delta x_{i-\frac{1}{2}}}\phi^{x+}_{i-\frac{1}{2},j,k}\right.$$
$$\left.+\frac{1}{2}\left(1-\frac{\Delta t u^{+}_{i+\frac{1}{2},j,k}}{\omega_{i+\frac{1}{2},j,k}\Delta x_i}\right)\frac{\Delta x_i}{\Delta x_{i+\frac{1}{2}}}\frac{\phi^{x+}_{i+\frac{1}{2},j,k}}{r^{+}_{i+\frac{1}{2},j,k}}\right)$$

$$A_{i,j+\frac{1}{2},k} = -\frac{\Delta t v^{-}_{i,j+\frac{1}{2},k}}{\omega_{i,j,k}\Delta y_j}\left(1-\frac{1}{2}\left(1+\frac{\Delta t v^{-}_{i,j+\frac{1}{2},k}}{\omega_{i,j+\frac{1}{2},k}\Delta y_{j+1}}\right)\frac{\Delta y_{j+1}}{\Delta y_{j+\frac{1}{2}}}\phi^{y-}_{i,j+\frac{1}{2},k}\right.$$
$$\left.+\frac{1}{2}\left(1+\frac{\Delta t v^{-}_{i,j-\frac{1}{2},k}}{\omega_{i,j-\frac{1}{2},k}\Delta y_j}\right)\frac{\Delta y_j}{\Delta y_{j-\frac{1}{2}}}\frac{\phi^{y-}_{i,j-\frac{1}{2},k}}{r^{-}_{i,j-\frac{1}{2},k}}\right)$$

$$B_{i,j-\frac{1}{2},k} = \frac{\Delta t v^{+}_{i,j-\frac{1}{2},k}}{\omega_{i,j,k}\Delta y_j}\left(1-\frac{1}{2}\left(1-\frac{\Delta t v^{+}_{i,j-\frac{1}{2},k}}{\omega_{i,j-\frac{1}{2},k}\Delta y_{j-1}}\right)\frac{\Delta y_{j-1}}{\Delta y_{j-\frac{1}{2}}}\phi^{y+}_{i,j-\frac{1}{2},k}\right.$$
$$\left.+\frac{1}{2}\left(1-\frac{\Delta t v^{+}_{i,j+\frac{1}{2},k}}{\omega_{i,j+\frac{1}{2},k}\Delta y_j}\right)\frac{\Delta y_j}{\Delta y_{j+\frac{1}{2}}}\frac{\phi^{y+}_{i,j+\frac{1}{2},k}}{r^{+}_{i,j+\frac{1}{2},k}}\right)$$

$$A_{i,j,k+\frac{1}{2}} = -\frac{\Delta t w^{-}_{i,j,k+\frac{1}{2}}}{\omega_{i,j,k}\Delta z_k}\left(1-\frac{1}{2}\left(1+\frac{\Delta t w^{-}_{i,j,k+\frac{1}{2}}}{\omega_{i,j,k+\frac{1}{2}}\Delta z_{k+1}}\right)\frac{\Delta z_{k+1}}{\Delta z_{k+\frac{1}{2}}}\phi^{z-}_{i,j,k+\frac{1}{2}}\right.$$
$$\left.+\frac{1}{2}\left(1+\frac{\Delta t w^{-}_{i,j,k-\frac{1}{2}}}{\omega_{i,j,k-\frac{1}{2}}\Delta z_k}\right)\frac{\Delta z_k}{\Delta z_{k-\frac{1}{2}}}\frac{\phi^{z-}_{i,j,k-\frac{1}{2}}}{r^{-}_{i,j,k-\frac{1}{2}}}\right)$$

DOI: 10.1002/fld

$$B_{i,j,k-\frac{1}{2}}=\frac{\Delta t w^{+}_{i,j,k-\frac{1}{2}}}{\omega_{i,j,k}\Delta z_k}\left(1-\frac{1}{2}\left(1-\frac{\Delta t w^{+}_{i,j,k-\frac{1}{2}}}{\omega_{i,j,k-\frac{1}{2}}\Delta z_{k-1}}\right)\frac{\Delta z_{k-1}}{\Delta z_{k-\frac{1}{2}}}\phi^{z+}_{i,j,k-\frac{1}{2}}\right.$$
$$\left.+\frac{1}{2}\left(1-\frac{\Delta t w^{+}_{i,j,k+\frac{1}{2}}}{\omega_{i,j,k+\frac{1}{2}}\Delta z_k}\right)\frac{\Delta z_k}{\Delta z_{k+\frac{1}{2}}}\frac{\phi^{z+}_{i,j,k+\frac{1}{2}}}{r^{+}_{i,j,k+\frac{1}{2}}}\right)$$

Define

$$R_{i,j,k}=\frac{1}{\omega_{i,j,k}}\left(\frac{-u^{-}_{i+\frac{1}{2},j,k}+u^{+}_{i-\frac{1}{2},j,k}}{\Delta x_i}+\frac{-v^{-}_{i,j+\frac{1}{2},k}+v^{+}_{i,j-\frac{1}{2},k}}{\Delta y_j}+\frac{-w^{-}_{i,j,k+\frac{1}{2}}+w^{+}_{i,j,k-\frac{1}{2}}}{\Delta z_k}\right)$$

and

$$S_{i,j,k}=\frac{u^{-}_{i+\frac{1}{2},j,k}u^{-}_{i-\frac{1}{2},j,k}}{\omega_{i,j,k}\omega_{i-\frac{1}{2},j,k}\Delta x_i^2}+\frac{u^{+}_{i-\frac{1}{2},j,k}u^{+}_{i+\frac{1}{2},j,k}}{\omega_{i,j,k}\omega_{i+\frac{1}{2},j,k}\Delta x_i^2}+\frac{v^{-}_{i,j+\frac{1}{2},k}v^{-}_{i,j-\frac{1}{2},k}}{\omega_{i,j,k}\omega_{i,j-\frac{1}{2},k}\Delta y_j^2}+\frac{v^{+}_{i,j-\frac{1}{2},k}v^{+}_{i,j+\frac{1}{2},k}}{\omega_{i,j,k}\omega_{i,j+\frac{1}{2},k}\Delta y_j^2}$$
$$+\frac{w^{-}_{i,j,k+\frac{1}{2}}w^{-}_{i,j,k-\frac{1}{2}}}{\omega_{i,j,k}\omega_{i,j,k-\frac{1}{2}}\Delta z_k^2}+\frac{w^{+}_{i,j,k-\frac{1}{2}}w^{+}_{i,j,k+\frac{1}{2}}}{\omega_{i,j,k}\omega_{i,j,k+\frac{1}{2}}\Delta z_k^2}$$

Since $\frac{1}{b}\varphi(a,b)\geqslant -2$ and

$$\frac{1}{b}\frac{\varphi(a,b)}{a}\leqslant 2$$

for all a,b, the coefficients $A_{i+\frac{1}{2},j,k}$, $B_{i-\frac{1}{2},j,k}$, $A_{i,j+\frac{1}{2},k}$, $B_{i,j-\frac{1}{2},k}$, $A_{i,j,k+\frac{1}{2}}$, $B_{i,j,k-\frac{1}{2}}$ are all nonnegative under (14), and

$$A_{i+\frac{1}{2},j,k}+B_{i-\frac{1}{2},j,k}+A_{i,j+\frac{1}{2},k}+B_{i,j-\frac{1}{2},k}+A_{i,j,k+\frac{1}{2}}+B_{i,j,k-\frac{1}{2}}\leqslant 2R_{i,j,k}\Delta t-\Delta t^2 S_{i,j,k}$$

Therefore, $c^{n+1}_{i,k,k}$ is a convex combination of $c^n_{i,j,k}$, $c^n_{i-1,j,k}$, $c^n_{i+1,j,k}$, $c^n_{i,j-1,k}$, $c^n_{i,j+1,k}$, $c^n_{i,j,k-1}$, $c^n_{i,j,k+1}$ as long as (12) holds with η defined in (15) or alternatively, $\eta=\frac{1}{2}$; the numerical scheme (13) is l^{∞}-stable and positivity preserving.

REFERENCES

1. GNR MoMaS webpage. Available from: http://www.gdrmomas.org/.
2. Bourgeat A, Kern M. Simulation of transport around a nuclear waste disposal site: the couplex test cases. *Computational Geosciences* (*Special Issue*) 2004; **8**(2).
3. Bruneau C-H, Marpeau F, Saad M. Numerical simulation of the miscible displacement of radionuclides in a heterogeneous porous medium. *International Journal for Numerical Methods in Fluids* 2005; **49**(10):1053–1085.
4. Choquet C. Radionuclide transport model with wells. *Asymptotic Analysis* 2004; **37**(1):57–78.
5. Chou CH, Li Q. Characteristics-Galerkin and mixed finite element approximation of contamination by compressible nuclear waste-disposal in porous media. *Numerical Methods for Partial Differential Equations* 1996; **12**(3): 315–332.

DOI: 10.1002/fld

6. Marpeau F. Analyse mathématique et numérique de phénomènes de transport réactif en milieu poreux et en dynamique des populations. *Ph.D. Thesis*, Université Bordeaux 1, 2005.
7. Marpeau F, Saad M. Mathematical analysis of radionuclides displacement in porous media with nonlinear adsorption. *Journal of Differential Equations* 2006; **228**:412–439.
8. Bear J. *Dynamics of Fluids in Porous Media*. Elsevier: Amsterdam, 1972.
9. de Marsily G. *Hydrogéologie Quantitative*. Masson: Paris, 2000.
10. Strang G. On the construction and comparison of difference schemes. *SIAM Journal on Numerical Analysis* 1968; **5**:506–517.
11. Roe PL. Generalized formulation of TVD Lax-Wendroff schemes. *ICASE Report*, 1984; 53–84.
12. Lascaux P, Théodor R. *Analyse Numérique Matricielle Appliquée à l'Art de l'Ingénieur*, vol. 1, 2. Masson: Paris, 1986–1987.
13. Bastian P, Lang S. Couplex benchmark computations obtained with the software toolbox UG. *Computational Geosciences* 2004; **8**(2):125–147.
14. Bourgeat A, Kern M, Schumacher S, Talandier J. The couplex test cases: nuclear waste disposal simulation. *Computational Geosciences* 2004; **8**(2):83–98.
15. Chénier E, Eymard R, Nicolas X. A finite volume scheme for the transport of radionuclides in porous media. *Computational Geosciences* 2004; **8**(2):163–172.
16. del Pino S, Pironneau O. Asymptotic analysis and layer decomposition for the couplex exercise. *Computational Geosciences* 2004; **8**(2):149–162.
17. Hoteit H, Ackerer PH, Mosé R. Nuclear waste disposal simulations: couplex test cases. *Computational Geosciences* 2004; **8**(2):99–124.
18. Trujillo D. Mixed primal–dual method for nuclear waste disposal far field simulation. *Computational Geosciences* 2004; **8**(2):173–185.
19. Godlewski E, Raviart PA. *Hyperbolic Systems of Conservation Law*. Ellipses: France, 1990.
20. Bruneau C-H, Fabrie P, Rasetarinera P. An accurate finite difference scheme for solving convection-dominated diffusion equations. *International Journal for Numerical Methods in Fluids* 1997; **24**(2):169–183.
21. Sweby PK. High resolution schemes using flux limiters for hyperbolic conservation laws. *SIAM Journal on Numerical Analysis* 1984; **21**(5):995–1011.

DOI: 10.1002/fld